MASTER'S THESIS

Study of stimulated emisson from light emitting polymers

Chan, Kin Long

Date of Award:
2015

Study of Stimulated Emission from Light Emitting Polymers

CHAN Kin Long

A thesis submitted in partial fulfillment of the requirements

for the degree of

Master of Philosophy

Principal Supervisor: Prof. CHEAH Kok Wai

Hong Kong Baptist University

Aug 2015

DECLARATION

I hereby declare that this thesis represents my own work which has been done after registration for the degree of MPhil at Hong Kong Baptist University, and has not been previously included in a thesis or dissertation submitted to this or other institution for a degree or other qualifications.

Signature:_____

Date: Aug 2015

ABSTRACT

Efficient and high light amplification of optical resonator in organic laser is one of the critical factors for high performance organic laser. It can be achieved by using microcavity and DFB structures, which are commonly adopted methods to enhance light amplification in specific wavelength. Both of them are the more widely used structures in inorganic and organic lasers. In this work, we employed nearly 100% reflection (at 450 nm) DBR and Al to act as reflected mirror inside the microcavity device. The function of microcavity has been examined to show the ability of device in tuning laser emission wavelength and overcoming the loss of organic-metal interface. DFB structure was used to demonstrate different laser emissions with respect to different grating periods. The finding clarifies the role of the structure in enhancement of light amplification leading to lower threshold, which was half of that of amplified spontaneous emission from single layer of PFO. As designed laser mode is also an important factor to get a high performance organic laser, those laser modes of structures have been designed and estimated by simulations and consistent with the experimental results.

Color tunable light source has great potential for display, lighting and bio-imaging. Current broadband light sources, however, have their own limitations in beam divergence and device size. In this work, we demonstrated a spatially variant light source with tunable color emission property by using two cascaded organic thin films, which emit blue and green ASE respectively under optical pumping. By spatially selecting the overlapping of the directional ASE from the cascaded films, we show that the color of light emission can be continuously tuned from blue, white to green.

ACKNOWLEDGEMENTS

I would like to send my thankfulness profoundly to my supervisor, Prof. K.W. Cheah for his guidance and advice during the study period. His patience and generous in accepting all my demerits are appreciatively acknowledged. I am also grateful to have an opportunity to participate in different projects, which broaden my horizon in the various research fields.

I would also like to express my sincerely thanks to my co-supervisor, Dr. G.X. Li, for his comments and concern to my studies. His guidance is of paramount importance during the experiment. Thanks are also given to Dr. S.M. Chen for her assistance in the SEM experiments, and Mr. P.L. Tse for his technical support in the equipment operation.

Sincere thanks are also given to my co-workers in IAM, namely, Dr. H.L. Tam, Dr. K.F. Li, Miss C.M. Chow, Dr. S.Y. Ching, Miss. Y.W. O, Miss K.M. Fung, Mr. K.C. Tam, Dr. C. Cai, And Mr. W.Y. Lam. They assisted me to finish all my experiments successfully by sharing their research experience and knowledge.

Also, I would like to take this chance to thank all my friends in Physics Department and other Departments for providing me a pleasant and happy study period.

Last but not least, I would like to thank my family, grandmother, father, mother, brother and Emily Chong for support, patience and encouragement throughout my study.

TABLE OF CONTENTS

LIST OF FIGURES

LIST OF TABLES

CHAPTER 1 INTRODUCTION TO LIGHT AMPLIFICATION

1.1 History and development of light amplification

We live in an instant information world. This is supported by the advance in electronic technology leading to better live with positive impact to us. However, the resources and methodologies used to manufacture that electronic raise serious problems arising from negative environmental impacts of the manufacture, such as use and disposal of electronic devices. Thus, the use of organic materials including small molecules and polymers to construct the novel electronic devices can offer a more environmental friendly and affordable world. Also, organic light amplification is included to be a promising organic electronic device.

In 90s, the first demonstration of lasing in organic conjugated polymer showed that the materials have the ability for lasing and possibility to have organic lasers [1]. Further development in few years later, the first solid-state optically pumped organic polymer laser was demonstrated [2].Since that, the great interest in organic semiconductor lasers has rapidly increased. There are in a number of research articles in this field [3-5] in the following years. Moreover, the organic lasers have been demonstrated by using several of designed resonators, including microcavities [6-8], distributed feedback [9-10], and microrings [11].

The first solid-state organic polymer lasing was demonstrated under optical pumping. And it was using simple waveguide structures to produce low gain narrowing threshold in organic thin films. After that several more polymers were used in the waveguide structures showing the ability for lasing. The simple waveguide structures with polymers and suitable substrate (e.g. fused silica) also exhibit Amplified Spontaneous Emission (ASE). Hence, ASE with simple waveguide

structures is commonly used to examine the gain coefficient of materials. It allows the identification of variations in materials inherent behavior, rather than the effect of the resonant cavity. Moreover, these studies allow establishing structure-property relationships that provide important clue to scientists for the improvement of materials design for lasing. The most importance of ASE is that it is very similar to lasing, and it is the first step to develop organic laser and we will discuss the similar and difference between ASE and laser later in Section 2. Fig. 1.1 showed the recent research in ASE using pervoskites fabricated from solution process [12]. In their work, they showed optical gain of the materials and also wavelength tunable ASE for further development in laser.

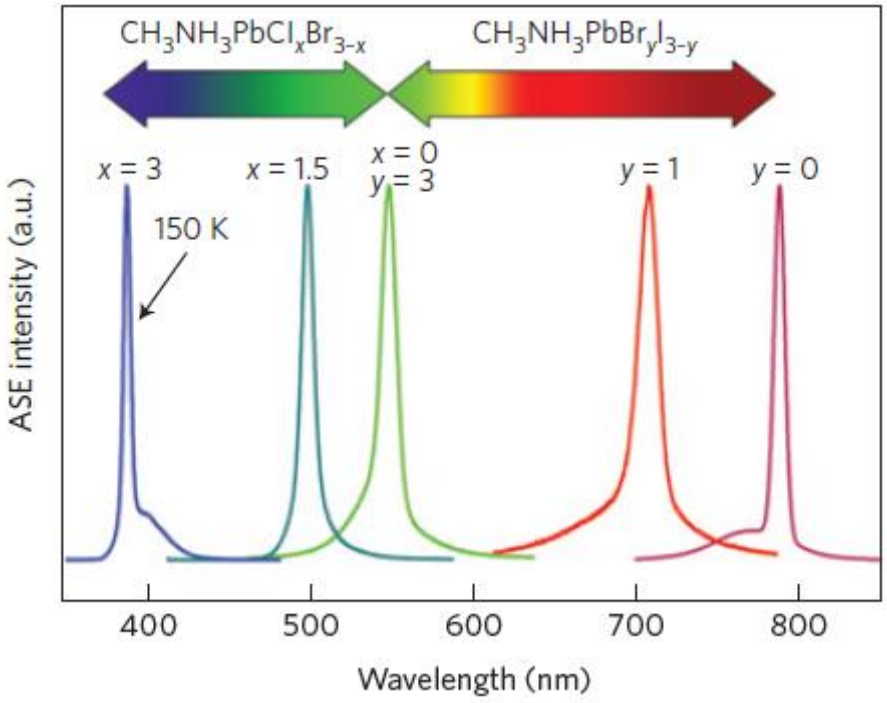

Fig.1.1 Wide wavelength tunability of ASE wavelengths from low temperture solution processed perovskite films [12].

Apart from the simple waveguide structures for lasing, various optical resonators were employed to demonstrate organic laser. The microcavity and distributed feedback structures are mostly employed in organic lasers. The first organic

semiconductor laser was based on Fabry-Perot microcavities to provide optical feedback, with the organic materials in solution or solid state [1-2]. When a gain medium is placed within a Fabry-Perot oscillator with gap matching that of the medium emission wavelength, an active micocavity is formed. Due to the high values of optical gain of organic polymers, a layer of only nanometer order of thickness was required inside the cavity to achieve laser. Emitted light from cavity is coupled to the cavity modes resulting in narrowing and a degree of control over the emission. An advantage of the microcavity design is the ease of fabrication and the emission is perpendicular to the substrate. Also, distributed Bragg reflector is among the most commonly used design of microcavity; it consists of the gain medium surrounded by alternating layers of high and low refractive indices. The strong reflection caused by the reflector would increase the Q-factor improving the light amplification.

The incorporation of periodic structure into a polymer waveguide device provides the geometry required for a distributed feedback laser. This is a periodic change in the refractive index for optical feedback. Distributed feedback lasers were introduced in the 1970s [13] and further development in coming years, such as 2D gratings [9] and circular gratings [14]. By varying the film thickness or period of the grating allows the emission wavelength to be varied. Fig.1.2 showed the real time tunable lasing from plasmonic nanocavity arrays [15]. This recent research employed both cavity and grating structures, achieving dynamic tuning of the Plasmon lasing wavelength.

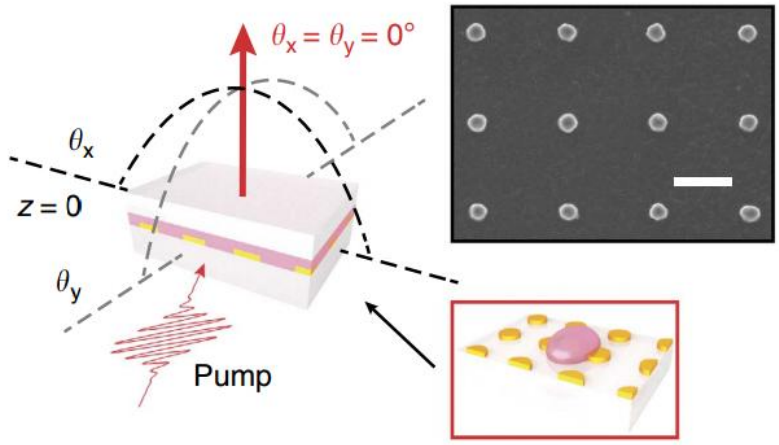

Fig.1.2 Scheme of a lasing device and SEM image of Au NP arrays.History and development of light emitting polymers[15].

1.2 History and development of light emitting polymers

The main advantage of using organic semiconducting polymer to construct the lasers is the high values of optical gain with broaden gain spectral bandwidth of the materials. Also the flexibility of synthesis makes that the output emission can be tunable among the whole visible range [16, 17-19]. However, the excitation of organic semiconducting polymer lasers can only be done under optical pumping. The obstacle for being electrical pumping is mainly due to the low charge mobility of the materials [16, 20-21]. Thus, many scientists are still studying the organic lasers in achieving the electrical pumping, and mainly focus on two aspects; first is materials development improving the optical properties of materials to make light emission more efficient. The second way is lowering the threshold of laser emission using better optical resonators.

The key advantages of polymers are easy to process, conducting and flexibility of synthesis. These lead to cheaper and large amount of production making that the materials draw more and more attentions and studies in both industry and laboratory.

In 1977, the first report on electrical conductivity in the organic polymer materials was synthesized by Shirakawa et al [22-23]. In 2000, to acknowledge the importance of the new type materials, they are awarded the Nobel Prize in Chemistry for the discovery and development of conductive polymers [24]. The discovery of conductive polymers initiates an intense research in these materials ever now. In Table 1.1, there are some samples of light emitting polymers.

IUPAC Name	Abbreviations	Chemical structure
Polymer Materials		
Poly(9,9-di-*n*-dodecylfluorenyl-2,7-diyl)	PFO	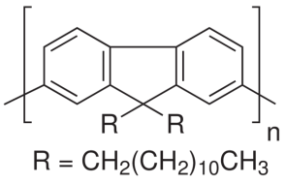
Poly[(9,9-di-*n*-octylfluorenyl-2,7-diyl)-*alt*-(benzo[2,1,3]thiadiazol-4,8-diyl)]	F8BT	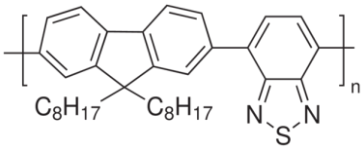
Poly(3-hexylthiophene-2,5-diyl)	P3HT	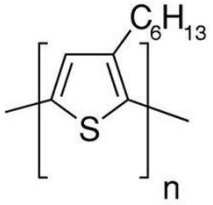
Poly[2-methoxy-5-(2-ethylhexyloxy) -1,4-phenylenevinylene]	MEH-PPV	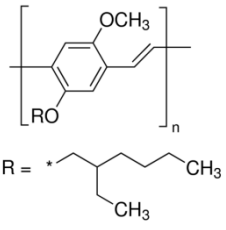

Table.1.1 Examples of Polymer Materials [16].

In the past few decades, organic polymer materials have been applied in organic light emitting diodes [25-29], organic solar cells [30-31], photo detectors [32-33], and

organic transistors [34-36]. Fig.1.3 showed various polymer laser resonators including microcavity, microring and distributed feedback laser [5]. The above described organic applications are well developed following the inorganic counterparts; some of them have even already produced into commercial products. However, the organic light amplification or lasers are still in research stage.

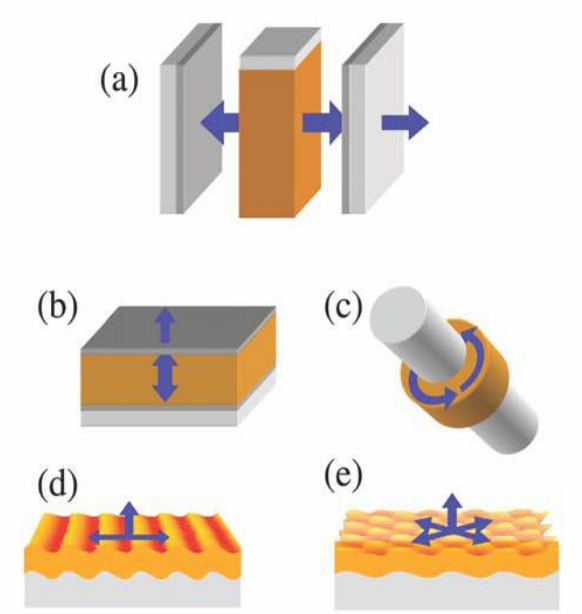

Fig.1.3 Schematics of various polymer laser resonators [5].

1.3 Research focus

This work focuses on the organic laser design, fabrication and development of measurement and uses different optical resonators to improve the organic semiconducting laser. The optical properties of organic semiconductor lasers are demonstrated and show how improvements can be made in the optical pumping. The light amplification of organic thin films is first investigated with a novel idea to create a tunable color of amplified spontaneous emission. Distributed feedback structure and microcavity structure are also employed to demonstrate organic semiconducting lasers by optical pumping. The better performance is expected using these optical resonators.

CHAPTER 2 THEORY OF LIGHT AMPLIFICATION

In this chapter, the background theory of light amplification in organic semiconductors is discussed, including the amplified spontaneous emission and organic polymer laser. It will describe both electrical and optical properties that make them being promising as an organic laser. In polymer laser, different device structure of organic laser will be presented.

2.1 Introduction

In this chapter, the theory of light amplification in organic semiconducting (conjugated) polymer will be focused. The light amplification, in this research, can be separated into two parts, the amplified spontaneous emission (ASE) and laser. The mechanism of amplification spontaneous emission is similar to laser, both having spectra narrowing and clear threshold [37-40], but it is not lasing. Because it can only provide a limited degree of coherence and monochromaticity, also the laser resonator does not strongly influence the emission [41]. Laser is an acronym that stands for “Light amplification by stimulated emission of radiation”. ASE and laser both consists of three parts, a pumping source (laser) for providing photon energy to the sample, a gain medium (mostly organic semiconducting polymer in this work) for processing the optical gain and experience the light amplification and a resonator for amplifying light in gain medium. Nevertheless, the resonator is the critical difference to identify two of them in this study. The ASE can be achieved from neat thin film on planar substrate, while lasing would need various structures, such as distributed feedback structure and cavity structure. The electrical properties of organic semiconducting polymers will be first to discuss and explains why it is so promising for electrical pumping which is a big mile stone for organic laser.

2.2 Electrical properties

Since organic semiconducting polymer was discovered, these materials open the possibility of electrical conducting organic devices including electrically pumped organic laser [42, 43]. Those materials have the properties of electrical conductivity, light emission and capable for charge transport. However, there are still challenges to be overcome for electrical pumping, such as lower threshold is needed, reducing the losses in layer absorption and the shorter excited-state lifetime of materials [16]. Nevertheless, organic semiconducting polymer is still promising materials to develop electrical pumped organic laser. Because they compared with other organic materials, like dyes, they showed higher photo-stability and without PL quenching [44].

2.3 Optical properties

The optical properties of organic semiconducting polymer are determined by their electronic state, the lowest unoccupied molecular orbital (LUMO), highest occupied molecular orbital (HOMO) energy levels and the energy difference between both levels (band gap) [45]. These energy levels correspond to valence and conduction bands in inorganic semiconductors. In optical characteristics, they mostly have broad photoluminescence spectra, strong absorption coefficients and have a wide range of color in visible light [46]. And those properties are strongly depending on energy levels inside the polymers, so it opens various directions for scientists to synthesis different molecular structure for light emitting across the visible spectrum.

2.3.1 Absorption and emission

When incident light excited the organic semiconducting (conjugated) polymer molecule, absorption of photon energy which is matched to the energy gap (in conjugated polymer, like PFO (Poly(9,9-di-n-octyfluorenyl-2,7-diyl)), is π and π^* levels). After that the electrons are pumped from ground to the electronically excited state, and leave holes behind with a positive charge. The electron and hole are

bounded together by the Coulomb's law forming excitons [45, 47]. That is the main mechanism of optical transition inside organic semiconducting materials.

The Franck-Condon principle can be used to explain the whole picture of absorption and emission [48-50]. The principle states that during an electronic transition, a change from one vibration energy level to another energy level will be more likely to happen if the two vibrational wave functions overlap more significantly. In Fig.2.1, the inside electronic transitions are shown. The energy of photon is absorbed by molecule; the electron is excited from the ground vibration state (S_0) and moving to the excited vibrational state (S_1). Due to the time of absorption of light ($\sim 10^{-15}$ s) is much faster than molecular vibration ($\sim 10^{-12}$ s), the transition is alike vertical transition in figure (0-1 transition).

Principle of emission is similar to absorption, using Franck Condon principle again. When the molecules are excited to higher energy state (S_1), they will relax to lowest energy state (S_0) quickly (1-0 transition). The emission light is called fluorescence. There is a clear Stokes' shift between the absorption and emission spectra due to the molecule positions changed, and thus a red-shift from absorption is observed. Because of the energy difference of both spectra, it enhances the efficiency of emission by decreasing self-absorption.

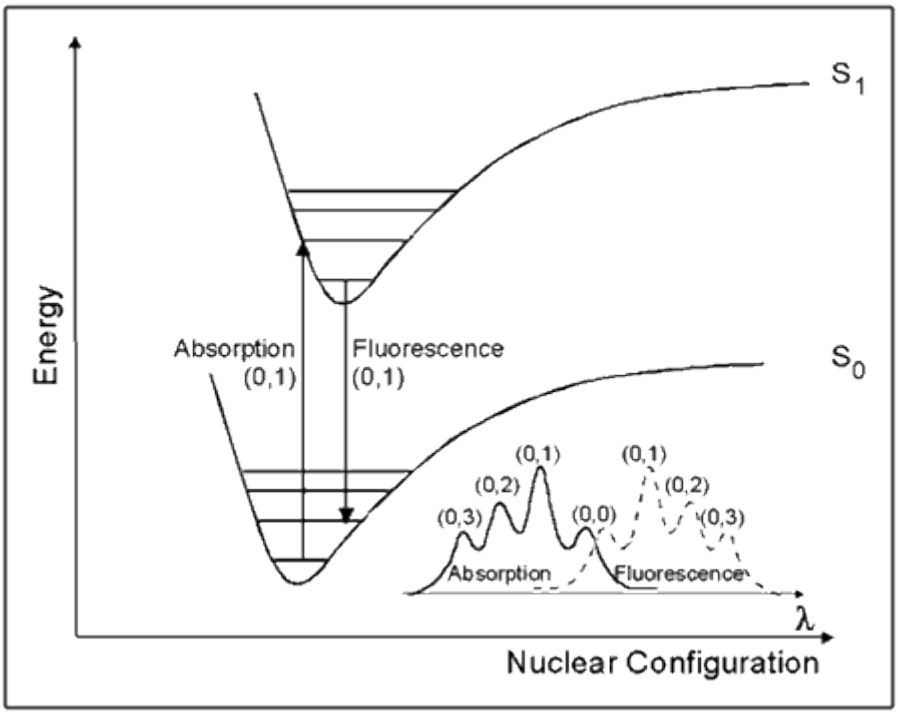

Fig.2.1 Franck Condon energy level diagram[51]

2.3.2 Gain in polymer

Organic semiconducting (conjugated) polymer is employed to be gain medium in laser resonator to produce the stimulated emission. And the gain can be explained by Section 2.3.1. Stimulated emission will be occurred after absorption. The details of stimulated emission will be discussed in Section 2.3.3. The gain mechanism in polymer can be well expressed by four-level energy scheme, especially for the conjugated polymer [45, 52]. The energy level diagram for gain medium is shown in Fig.2.2.

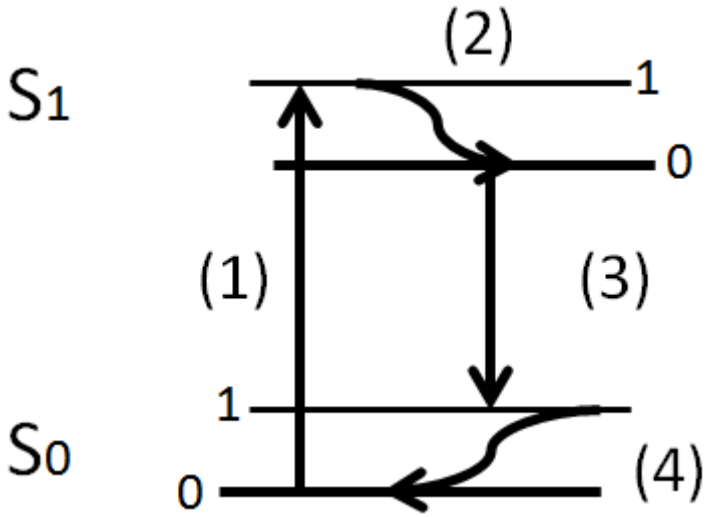

Fig.2.2 Four-energy level diagram for gain medium

A four-level energy system of gain medium is suitable and capable for lasing. To achieve stimulated emission, the population inversion is needed. Population inversion implies that more electrons excited to the higher energy state than in the lower energy state. By using four-level energy system, the population inversion can be easier to occur and the threshold for lasing is lower. We focus on transition (3) in Fig.2.2 for lasing and population inversion takes place at its upper energy level and lower energy level but not the highest energy level and ground state. Thus, the population inversion can be much easier to achieve even though most electrons are in the ground state [53]. As a result, the organic semiconducting (conjugated) polymer is promising to be a gain medium for lasing.

2.3.3 Spontaneous and stimulated emission

In order to study the processes for light amplification in gain medium, a simple two-level energy system was described in Fig.2.3. Inside this system, mainly three different processes may induced, stimulated absorption: spontaneous emission and stimulated emission.

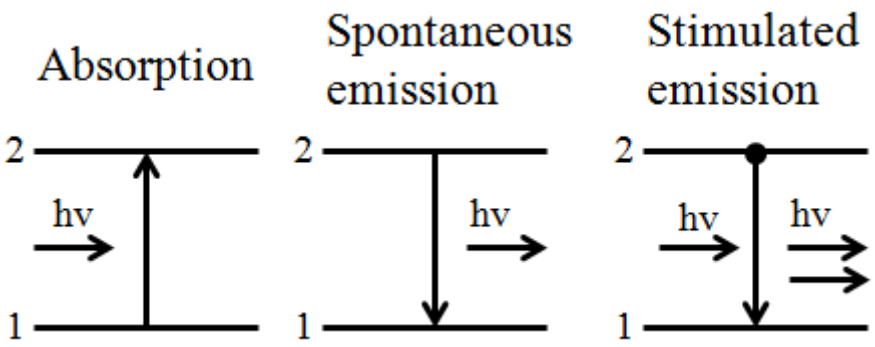

Fig.2.3 Two-levelenergy system with three processes

In Fig.2.3, the system has two energy levels E_1 and E_2, and population density N_1 and N_2 respectively. First of all, the stimulated absorption meant that there is incoming photons which are absorbed by the molecules. The photon energy is hν = E_2-E_1. An upward transition by the electrons will take place ($E_1 \rightarrow E_2$). The Rate of electrons in this transition can be given as [53-55]:

$$dN_1/dt = -N_1 B_{12} u(\nu_0) \qquad (2.1)$$

, where B_{12} is Einstein coefficient for absorption, $u(\nu_0)$ is the photon density and the negative sign is because of decreasing of population in that level.

After absorption, electrons are excited to the higher energy level (E_2). The electrons at the upper state then spontaneously fall to lower state (E_1) and emit a photon, and that is called spontaneous emission. Because of random or spontaneously relaxation, the emission is incoherence. That is the wave function having the random phase differences.

The total rate at this transition between two levels is:

$$dN_2/dt = -N_2 A_{21} \qquad (2.2)$$

, where A_{21} is Einstein coefficient for spontaneous emission and also is the inverse relationship of nature lifetime of electron.

After absorption, there is another possible may occur, stimulated emission. Induced by incident photon, the electron moves to higher energy level (E_2), and go down to lower energy level (E_1), thereby emitting an extra photon to join with the initial photon. Both of photons are in same phase, energy and frequency. The rate of the transition from E_2 to E_1 is shown as:

$$dN_2/dt = -N_2 B_{21} u(\nu_0) \qquad (2.3)$$

, where B_{21} is Einstein coefficient for stimulated emission.

Using Equation 2.1 to 2.3, we can tell that amplification of light can be achieved by stimulated emission and of course population inversion is needed (population of $E_2 > E_1$). But in this two-level energy system, most of molecules are at lower energy state. Even when the incident light has high intensity to make rate of stimulated emission higher than absorption and population inversion is satisfied, the high intense light may cause damage of the materials and loss of lasing. Thus, as mentioned in Section 2.3.2, the 4-level energy system in organic semiconducting (conjugated) polymer is more appropriate to be the gain medium for organic laser.

2.3.4 Amplified spontaneous emission

Amplified spontaneous emission will take place if the population of electrons from ground state is raised to the upper level is very high and the gain medium is optically dense. For this phenomenon to take place we can consider the situation in Fig.2.4 which can generate intense radiation without an optical cavity; however, it has limited gain.

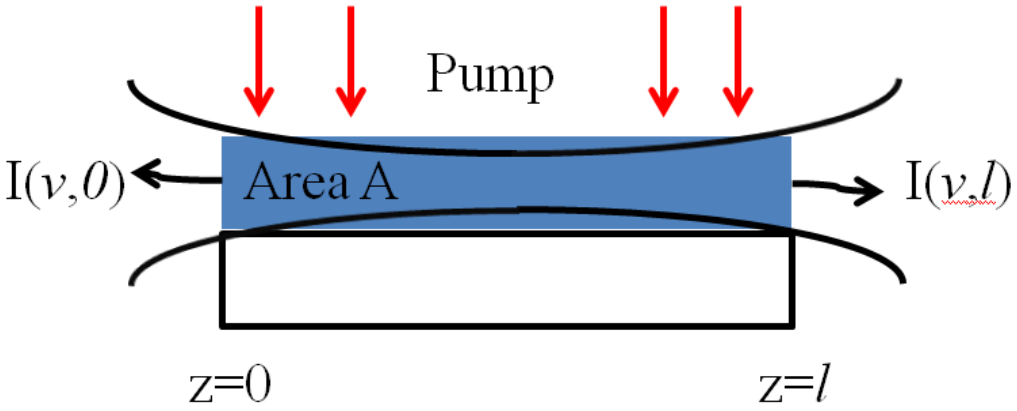

Fig.2.4 Schematic diagram of optical amplifer

In Fig.2.4, an optical amplifier is pumped by a light source (mainly a laser). For convenience of calculation, there is only considering one direction of light from z =0 to z= *l*. Inside the gain medium, the excited atoms will relax spontaneously, that is spontaneous emission. However, when the excitation energy is high enough to achieve a net gain in amplifier, the stimulated emission will take place. The intensity of the emission which is propagating along the z-axis in Fig. 2.4 can be obtained by [53-55]:

$$\frac{d}{dz}[\mathrm{I}(\nu,z)\,\mathrm{d}\,z]=\gamma(\nu)\,\mathrm{I}(\nu,z)\,\mathrm{d}\,z+\mathrm{h}\,\nu\,\mathrm{A}_{21}\,\mathrm{N}_{2}\,\mathrm{g}(\nu)\,\mathrm{d}\,\nu\frac{d\Omega}{4\pi} \quad (2.4)$$

, where I(*v*, *z*)is intensity of radiation, $\gamma(\nu)$ is net gain for the stimulated emission, A_{21} is Einstein coefficient for spontaneous emission, g(*v*) is net gain for the spontaneous emission, N2 is the population density, and $\frac{d\Omega}{4\pi}$ is the solid angle which is related to the film thickness and the length of the excitation area.

It describes that a radiation I(*v*, *z*) travels along the z-axis, with a constant solid angle $\frac{d\Omega}{4\pi}$. Between z=0 to z=l, the spontaneous emission is increased along this direction; stimulated emission also amplifies the intensity of the out coming light in

this lengths. On the right hand side of Equation 2.4, the first part is representing the stimulated emission intensity and the second part is contributed by the spontaneous emission. A solution to Equation 2.4, it is given by [53-55]:

$$\mathrm{I}(v, z = l) = \frac{\mathrm{h}\, v\, \mathrm{A}_{21}\, \mathrm{N}_2\, \mathrm{g}(v)}{\gamma(v)} [\exp(\gamma(v) l) - 1] \frac{d\Omega}{4\pi} \quad (2.5)$$

From Equation 2.5, we know the contributing sources in intensity of ASE. [53, 56-59] As the ASE contains both spontaneous emission and stimulated emission, ASE is incoherence light. Other parameters are directionality and spectrum narrowing [37-40, 59-62]. Since Equation 2.5 showed that the intensity of the ASE is a function of wavelength, i.e. light of the specific wavelength, was amplified into a high intensity.

ASE is very similar to lasing. Both are having spectral narrowing, directional emission and threshold of pumping energy. However, there are some differences between them: first, lasing is coherence light and ASE is not. It is because that ASE consists both spontaneous and stimulated emissions. And the other difference is higher threshold energy is required in ASE since ASE can occur without any optical cavity.

2.4 Polymer laser

After investigating the optical and electrical properties of organic semiconducting (conjugated) polymers, in this section, we will introduce different methods to manipulate the light emission to enhance the light amplification. Many methods are employed for enhancement of polymer laser. And we will mainly discuss these three: distributed feedback structure [24, 63], microcavity structure [21] and a simply neat film on substrate acting as waveguiding [32, 39, 58, 59].

2.4.1 Waveguiding

Optical waveguiding is useful to amplification of the light leading to lasing. The simplest waveguide can be the organic polymer as the gain medium and spin-coat on the fuse silica substrate. One of the condition in the optical waveguide is $n_a < n_s < n_p$, where n_a, n_s, and n_p are the refractive indices of air, substrate and polymer respectively [64]. In optical waveguides, light is channeled by the total internal reflection along the interface of different media. These light confines together to amplify the intensity. The modes inside the optical waveguide is strongly depends on the refractive index and thickness of the waveguide. [64-66]

2.4.2 Distributed feedback laser

Distributed feedback (DFB) lasers are well studied in past decades. It is using of periodic nano-structure to provide an optical feedback to enhance the light amplification. In early 70s, the DFB lasers were demonstrated with gain medium and the DFB interference patterns employed [67]. Later, organic semiconducting polymers were firstly employed as a gain medium and 2D grating was also fabricated [63, 68]. The DFB lasers are promising and attractive that many parties are investigated in this [24, 51-52]. The reasons are by using these structures the threshold can be decreased and emission wavelength can be tuned.

The fabrication steps of DFB laser is firstly spin-coating the thin film of organic semiconducting gain medium, such as polymer, onto the corrugated fused silica substrate. There are several fabrications techniques of the corrugated fused silica substrate, for example, nano-imprint lithography, electron beam lithography, soft lithography, and ink-print lithography [73-76]. The basic idea of the laser is that the light is creating an optical confinement in high refractive index gain medium (comparing to refractive index of air and substrate) through reflection by the periodic corrugations. By using the suitable periodic grating, the reflected light from each

grating can be combined by constructive interference, known as Bragg scattered. Those light reflected by the corrugation, will confine the light within the medium resulting in either ASE or stimulated emission. The DFB laser is strongly depending on frequency and resonant mode that is needed to satisfy to the Bragg condition:

$$m\lambda_{Bragg} = 2n_{eff}\Lambda \quad (2.6)$$

, where *m* is an integer of the order of the diffraction, λ_{Bragg} is the wavelength of the light, n_{eff} is the effective refractive index of the whole structure, and Λ is the periodicity of the grating. Moreover, the incident light has an incident angle (Fig.2.5) and Equation 2.6 is modified:

$$m'\lambda_{Bragg} = n_{eff}\Lambda(\sin\alpha + \sin\beta) \quad (2.7)$$

, where α and β are the incident angle and reflected angle respectively.

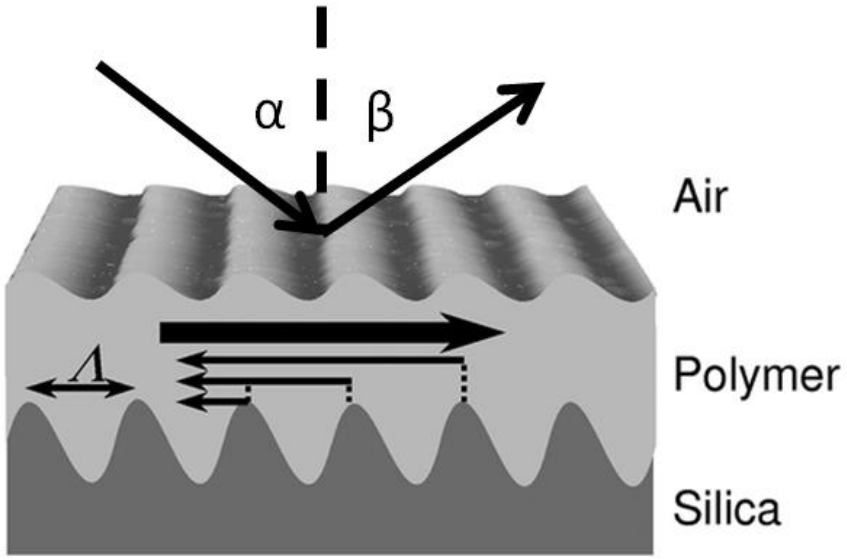

Fig.2.5 Diagram of 1-D distributed feedback structure [16]

Considering the incident angle to be 90^o, the β will also equal to 90^o and by calculating the reflected light which is providing a vertical-emitted output in first order of diffraction second-order Bragg reflection feedback. Different from Section2.4.1, DFB structure can dictate the output laser in vertical direction. Therefore it is possible to avoid the rough edge of the substrate of the waveguide and

scattering of the non-uniform edge. The structure also shows the ability to low the threshold usefully [68, 71, 77]. Apart from the one-dimensional of DFB structure, there is two-dimensional grating, and it can be considered by the superposition of two 1-D gratings having one rotating for 90^{o}. As a result, 2-D grating has a stronger light amplification leading to lower threshold of lasing. There is also three-dimensional grating but mainly for the random laser which is not our target, so we will not discuss about it.

2.4.3 Microcavity laser

The use of microcavity is common in light emitting devices. The design is sandwiching the organic semiconducting materials with two planar mirrors with a length of the order of the emission wavelength. The organic microcavity laser was first demonstrated at 1996 using two reflected mirror [21]. After that a number of related researches have been done [23, 78-82]. Inside the microcavity structure, the spatial distribution of spontaneous emission from gain medium is strongly modified by interference effects, and the total number of allowed photonic modes for spontaneous emission is reduced. After the decreasing of photonic modes, more of the photon emission is channeled into the lasing mode, which leading to more effectively increases the light emission cross section and highly reduces the pumping rate required to lower lasing threshold. The lasing mode is at the resonant wavelength, and the resonant wavelength is determined by the condition:

$$\lambda = \frac{2nL}{m} \quad (2.8)$$

, where n is the refractive index of gain medium, L is the cavity length, and m is an integer of the interference order [20, 53, 56]. Other advantages of this structure are the low-divergence and surface-emitted output.

In this study, we are using the microcavity structure with one metal mirror (Al)

and one Distributed Bragg Reflector (DBR) mirror. Distributed Bragg Reflector (DBR) is a structure formed by multiple layers of alternating materials with different refractive index. Each layer boundary causes a partial reflection of an optical wave, and these reflections combine with constructive interference, acting as a high performance of reflector. In a specific region of wavelengths, light can be nearly total reflected by the DBR mirror.

The reflectivity is given by [78]:

$$R_{2N} = \left(\frac{1 - \frac{n_l}{n_1}\left(\frac{n_2}{n_3}\right)^{2N}}{1 + \frac{n_l}{n_1}\left(\frac{n_2}{n_3}\right)^{2N}} \right) \quad (2.9)$$

, where n_l, n_1, n_2 and n_3 are the refractive indices of the air, the two alternation materials and the substrate and N is the number of repeated pairs of alternation refractive index materials. By increasing the number of pairs of the two alternation materials, the reflectivity can be increased. It would produce a high Q-factor of cavity, as the reflection in the wavelength can be relatively high (~100%).

CHAPTER 3 EXPERIMENTAL DETAILS

This chapter describes the materials, fabrication processes and different measurements which were used for this study. First, the polymer materials physical properties and chemical structures are introduced. And each step of experimental procedures will be presented, including cleaning and coating process. Also various measurements for characterization of device will be given.

3.1 Materials used

The chemical structures and physical properties of all polymer materials and solvent used in this study are showed in Table 3.1. The blue emission polymer PFO (Poly(9,9-di-n-dodecylfluorenyl-2,7-diyl) and green emission polymer F8BT (Poly[(9,9-di-n-octylfluorenyl-2,7-diyl)-alt-(benzo[2,1,3]thiadiazol-4,8-diyl)]) were employed as the active materials in this study. Those materials were purchased from Sigma-Aldrich. The molecule weight and polydispersity index of PFO are Mw $\leqq$ 20000 and ~ 3.7. The average molecule weight of F8BT is ~10000-20000 and polydispersity index is < 3.

IUPAC Name	Abbreviations	Chemical structure
Polymer Materials		
Poly(9,9-di-*n*-dodecylfluorenyl-2,7-diyl)	PFO	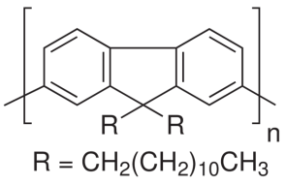
Poly[(9,9-di-*n*-octylfluorenyl-2,7-diyl)-*alt*-(benzo[2,1,3]thiadiazol-4,8-diyl)]	F8BT	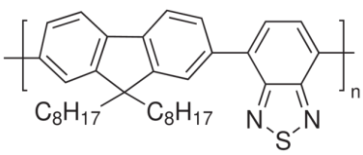

Solvent		
Methylbenzene	Toluene	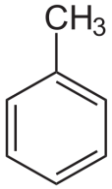

Table.3.1 Materials used

3.2 Substrate preparations

The sample used the synthetic quartz as substrates. The advantage of using synthetic quartz as substrate but not glass is that the transmittance can be higher in the ultraviolet region (Fig.3.1), since the excitation laser source used in experiment is in UV-zone (λ = 355 nm). The substrate size is 15 mm x15 mm and 1 mm thick and it can be easily covered completely by the polymer achieving better uniformity. Before the materials were spun on the substrates, the surface of the quartz should be well cleaned. This cleaning process and pre-treatment is important to ensure the sample quality.

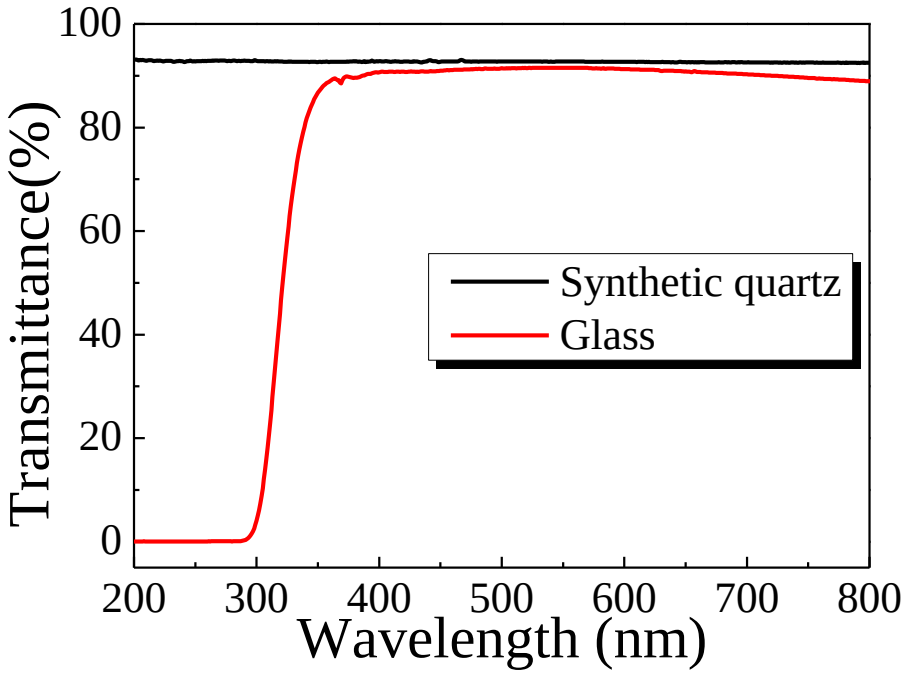

Fig.3.1.Transmittance of Synthetic quartz and glass

3.2.1 Cleaning procedures

The cleaning procedures are mainly using ultrasonic baths (Bransonic Ultrasonic Cleaner Model 1210) with Acetone, Ethanol and de-ionized water (DI water) repeatedly for each step at least 30mins. Acetone and Ethanol were used to remove the organic contaminants and dust on its surface and de-ionized water was used to remove those solvent and organic contaminants. Subsequently, the cleaned substrates were dried in the oven (Binder, Universal drying and heating ovens Model ED23-UL benchtop) at 110℃for least one hour or above to ensure both the moisture and solvents on the substrate surface have been removed.

3.2.2 Pre-treatment

For the pre-treatment, the cleaned substrates were subjected to oxygen plasma at 100W for 10 minutes to enhance the surface wetting on its surface. And the oxygen plasma treatment mechanism was shown in Fig.3.2 [84]. It will ensure that thin film coat on the substrate will be more smooth and uniform.

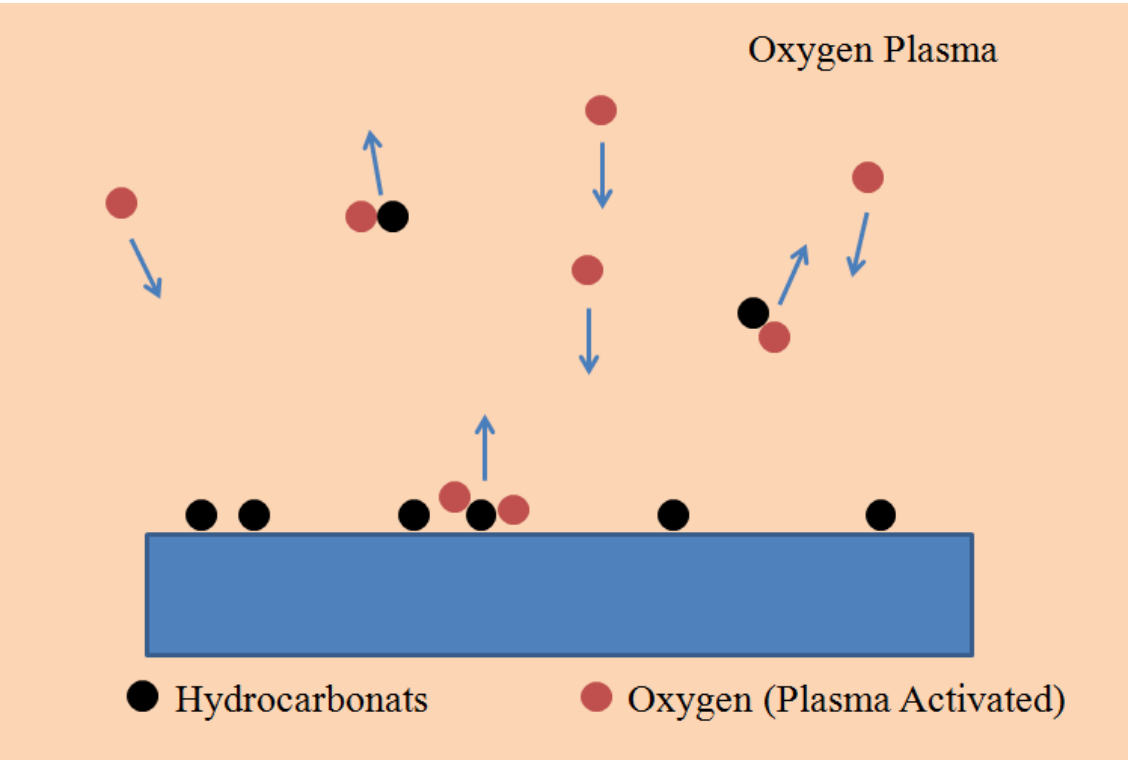

Fig.3.2.Oxygen plasma treatment mechanism

3.3 Fabrication

The fabrication was separated into two parts, spin-coating and thermal evaporation. Using two different methods for coating is due to the molecular weights of the polymer and small molecule materials.

3.3.1 Spin-coating

For spin-coating, we should first prepare the solutions. As PFO and F8BT are water-insoluble polymers, a water-insoluble liquid will be needed as a solvent. Toluene was used as solvent to make solution with those two materials. It can be used as solvent for a number of polymers. To prepare the solutions balance (OHAUS analytical plus balance) was used to determine the weight of materials, after that mixing with toluene to be a solution. Following that, the solution was heated by using the hotplate (RCT basic digital magnetic stirrer hot plate) up to 80℃ for 3 hours ensure that the polymer was totally dissolved in solution.

Spin-coating is widely used methods for polymer coating and can deposit relatively uniform and flat thin film. Since that polymer cannot be thermal evaporated, polymer layers of the sample were coated onto the substrates by spin-coating method. The equipment used was a spin-coater (Specialty Coating Systems Model P6700) as shown in Fig.3.3.

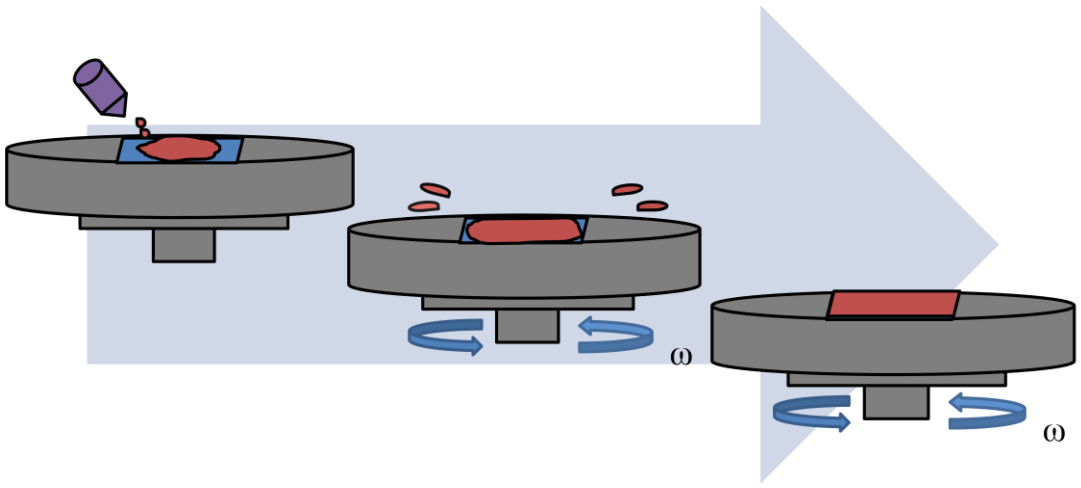

Fig.3.3.Diagram of spin-coater

It consists of two main parts, (1), the central point which provides a vacuum the suction to hold the substrate in place. (2), a spin accelerator that spins the sample. The processes are shown in Fig.3.1. At first, the solution of material was dropped on the prepared substrate. The solution was squeezed through a syringe filter of 0.45μm diameter for removing the large particle to ensure smooth surface formed on the sample. The substrate rotated at high rotational speed (in 2000RPM and 5s RAMP for 60 second), while higher angular speed usually get thinner thin film, also the viscosity of solution will affect the thickness of thin film too. After that the solution will spread out under the centrifugal force and formed thin film. Finally, the sample will put into a vacuum chamber for overnight to ensure that the solvent has been totally evaporated and to slow down photo oxidation, and then it is ready for experiment.

3.3.2 Thermal evaporation

For coating metal layers, such as Al and Ag, the thermal evaporation was used. The evaporator used is an eight-source Edwards's evaporator (Model Auto 306) as shown in Fig.3.4.

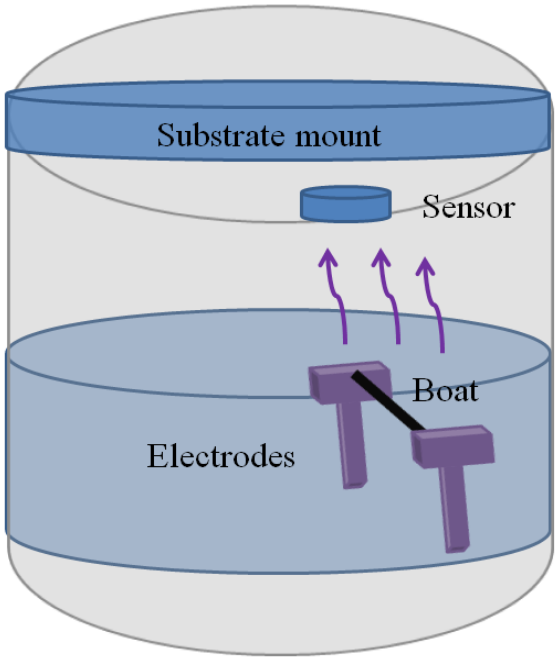

Fig.3.4.Diagram of thermal evaporator

It consists of two parts: 1) A substrate mount named numerically; 2) A base shutter with metal sources for separating materials and substrate. Each source has a pair of conducting electrodes and material evaporation boat, mainly using tungsten basket for metal. An external power supply was used to control the current passing through the material boat and obtained a desired deposition rate. The deposition rate and thickness were monitored by a crystal sensor. Controlling the coating rate of materials can tune the volume ratio of two materials coated in co-deposition process. In our experiment, those metals' deposition rates were around 2Å/s and the whole fabrication process was done in one pump down vacuum with pressure less than 6 x 10^{-6} torr.

3.4 Optical Characterization

For the optical characterization, several measurements were performed, such as spectra measurements combining some programmable measurement systems were used. Different measurement setups were needed as different stage of emissions, like fluorescence and lasing, will have difference of propagating directions.

3.4.1 Transmittance and Absorption measurement

The transmittance measurement of thin film was supported in the Chemistry Department of Hong Kong Baptist University. The sample absorption/transmittance was measured by a spectrophotometer (HP, UV-Visible Spectrophotometer Model 8453), and measuring range is between 190 nm to 1200 nm of wavelength.

3.4.2 Fluorescence measurement

Photoluminescence (PL) spectra of thin films were measured using He-Cd laser (wavelength: 325 nm) as the excitation source. The resulting photoluminescence is recorded by monochromator(SpectraPro-500i). After processing, the data is received

across different wavelengths from 350 nm to 800 nm.

3.4.3 ASE measurement

Amplified spontaneous emission is an essential phenomenon for testing the suitability of materials for lasing. When optically pumped, the material can undergoing the population inversion, ASE would appear with spectrum narrowing when the pumping power above the threshold. Investigation of ASE in different materials and its properties, the easiest and common method is to perform optical pumping the material in solid thin film.

For ASE measurement, the Ocean Optics (USB 4000-UV-VIS) was used and the optical path from the laser and sample to the Oceans Optics is also important. The thin film was pumped by a laser, Nd: YAG laser (Nd: YAG lasers Quantel Brilliant B) in 355 nm and 10 Hz. The laser will first be focused by convex lens. Following that cylindrical lens was used to transform the light into a rectangular shape beam or a line. Then an adjustable slit with 5 mm width was used to control the excitation area. And the excitation area was 5 mm x 300 μm. The setup was shown as Fig.3.5.

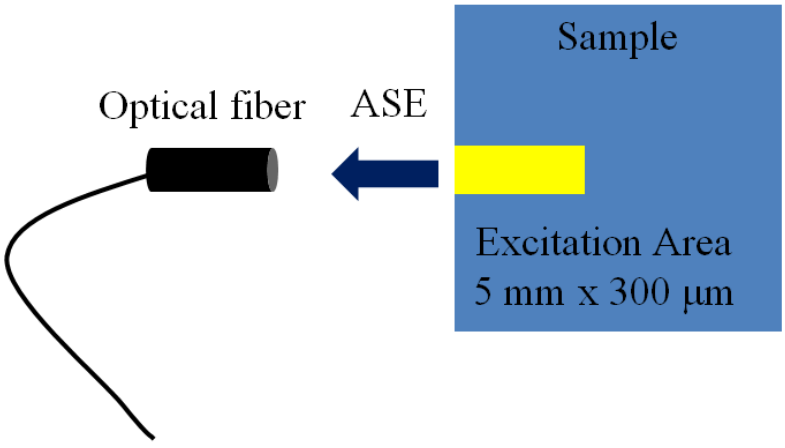

Fig.3.5. Schematic diagram of ASE measurement setup

The output light from sample came from the edge of sample, and used the convex lens to focus the output light. Though the fiber, the output light was collect to the Ocean Optics. Ocean optics is a spectroscopy system link with computer. It can

capture the spectra of the light from the fiber immediately. Then, it uses the averaging method to average spectra intensity in a period of time to calculate the spectra of the output light from sample.

3.4.4 Laser measurement

In laser measurement, all tested devices are distributed feedback laser or cavity laser. Distributed feedback laser is using a grating fused silica substrate and spin-coating the polymer materials onto the substrate; Cavity laser is using DBR-metal cavity with gain medium. The measuring setup is similar in section 3.4.3. However, due to different light propagation and device design, it will be some difference of the focus spot which is incident on the sample surface. For DFB laser, the measurement is using the same pumping source and was squeezed into rectangular beam but having relatively small size of excitation area (300 μm x 300 μm). For cavity laser, the same pumping source was focused into a small spot. Since all samples were chosen for surface emission, the pumping laser is incident with an angle onto the device surface. It is because the surface emitting laser beam from the device will not overlap with incident beam or photoluminescence from itself. With the incident angle, it is easier to detect the signal and observe the pattern and the measurement setup can be seen in Fig.3.6.

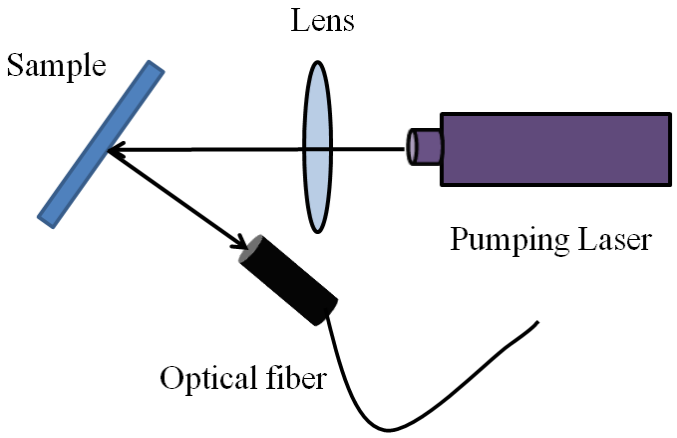

Fig.3.6. Laser measurement setup

3.5 Device Characterization

For the device characterization, several measurements were made to determine the device performance and characteristic. The high sensitivity and accuracy measurements were used, such as efficiency measurement and SEM measurements. Through those measurements, lasing properties can be further investigated.

3.5.1 Efficiency measurement

In order to determine the devices' efficiency and threshold, the energy efficiency of samples were measured. The Nd:YAG laser was used for this setup, because it is a suitable pump source for the selected materials. The setup is similar to Fig.3.6 but adding the reference power meter and is shown in Fig.3.7.

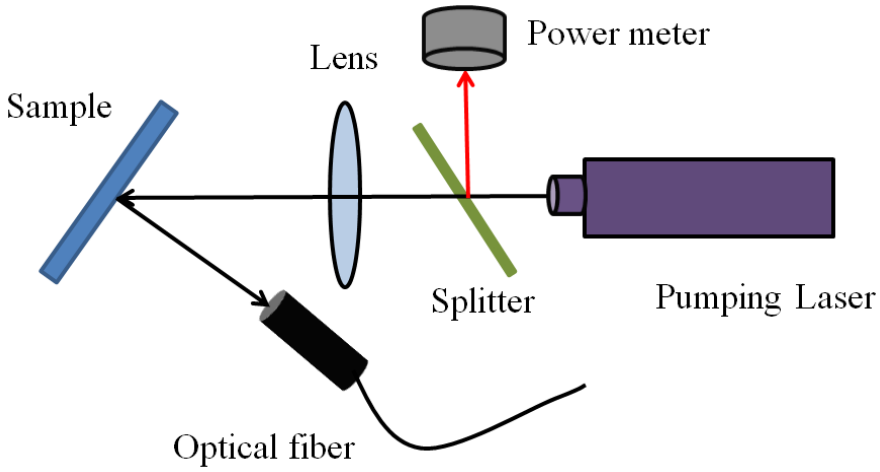

Fig.3.7. Efficiency measurement setup

In order to monitor the pump power, a splitter with splitting ratio around 15% to 85%was added to the setup. Firstly, we measured the power at position of sample and also the power of the light (red line in Fig.3.7) which is reflected by the splitter. The power of reflected light was selected to be a relatively lower power for estimating the original power that shining on sample. After that the sample was placed and by recording the relatively power. Then, we are able to receive the excitation power by calculation. Finally, the data of power meter was converted to energy unit. And by

combining the optical fiber system as the output intensity, the energy dependence can be obtained.

3.5.2 Ellipsometry measurement

Ellipsometry measurement is a useful optical technology for investigating the dielectric properties of thin films, including testing refractive index and dielectric function. Also, it can be used to characterize roughness, thickness and other material properties. It is used to measure the change in different polarization of reflection light from sample surface. The basic operating principle of this measurement is presented in Fig.3.8.

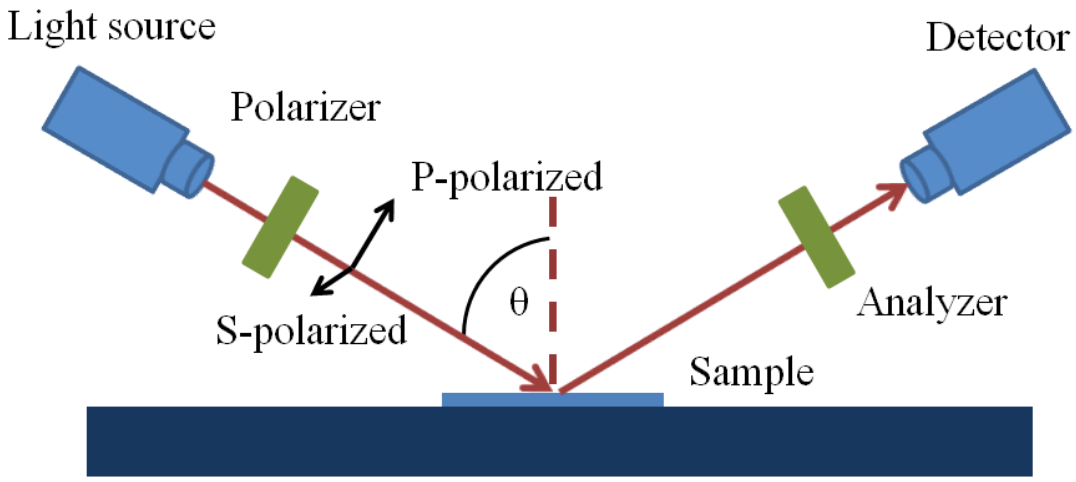

Fig.3.8. Ellipsometry measurement

Firstly, light emitted by a light source can be linearly polarized by a polarizer. It incidents onto the sample surface, and the reflected light pass through an analyzer and reach the detector. In this optical technique, the incident and reflection angle is set to be equal and both beams are polarized. The beams can be separated to two kind of polarizations: s-polarized and p- polarized, where s-polarized is the light polarization direction perpendicular to the plane of incidence and p-polarized is the light polarization direction parallel to the plane of incidence.

$$\rho = \frac{r_p}{r_s} = \tan(\psi) e^{i\Delta} \quad (3.1)$$

The equation 3.1 is used in ellipsometry system. It mainly include four Stokes parameters, named complex reflectance ratio, ρ, amplitude component, ψ , phase difference,Δ ,and the amplitudes of the s and p components, r_s and r_p. Because ellipsometry is only measuring the ratio of values, not the absolute value, it is accurate and reproducible methods. After collecting the raw data, they are converted into material's optical constants and thickness by using the ellipsometer in0house software. The software uses mainly Fresnel equations to derive those parameters.

For the experimental results, all of the thin film samples are deposited on the silicon wafer substrate, and the incident angle is set to 75^o. The major reason is the silicon wafer having a relatively high reflectivity comparing to glass substrate for getting higher reflective signal. By fitting the results, we can get the optical constants and thickness.

3.5.3 SEM measurement

A scanning electron microscope (SEM) is a powerful high-resolution(less than 1 nm) imaging system. It is a type of electron microscope using a focused electrons beam to scan sample that produces high quality images. Mainly, an interaction between electrons and atoms at or near the surface of sample generate signals that contain sample's surface info including topography and composition. SEM is operating in vacuum condition to ensure that the environment has no moisture and other gas molecules to interfere with the electrons or sample surface interaction. All samples must be electrically conductive to avoid charge built-up. For non-conducting sample, they have to be coated with metal film, usually gold, on sample surface by sputtering. In our experiment, the samples have silver-coated grating substrate, and can produce nano-scale images.

CHAPTER 4 TUNABLE COLOR EMISSION FROM CASCADED ORGANIC THIN FILMS

In this chapter, we showed a device consisting of two cascaded organic thin films, PFO and F8BT, emitting blue and green ASE respectively under optical pumping. By spatially selecting the overlapping of the directional amplified spontaneous emission form the cascaded films, we demonstrated the color of light emission could be gradually tuned from blue, white and green. The device performance results were analyzed, including lasing spectra, energy dependence and angle dependence.

4.1 Characterization of PFO and F8BT

PFO and F8BT are well established efficient light emission polymers [24-25, 80-82]. Thus, they were chosen in this work. To begin with, spin-coating conditions of the two polymers (in solution form) were determined, and basic optical characterization was measured.

4.1.1 Spin-coating condition of solution

As mentioned in Section 3.3.1, the sample thickness would be affected by the conditions of solution and the rotation speeds during spin-coating. The thickness dependence on the solution concentration of PFO and F8BT are shown in Fig.4.1 and Fig.4.2. With different concentrations of PFO or F8BT in the solvent, the film thickness varies. All of the samples were fabricated using the same spin-coat conditions, which was 2000 RPM and 5 second RAMP for 60 second. In Fig.4.1 and Fig.4.2, both of them show the linear relationship between thickness and concentration of the solutions. By using these relationships, the solution concentration could be determined for specific thickness.

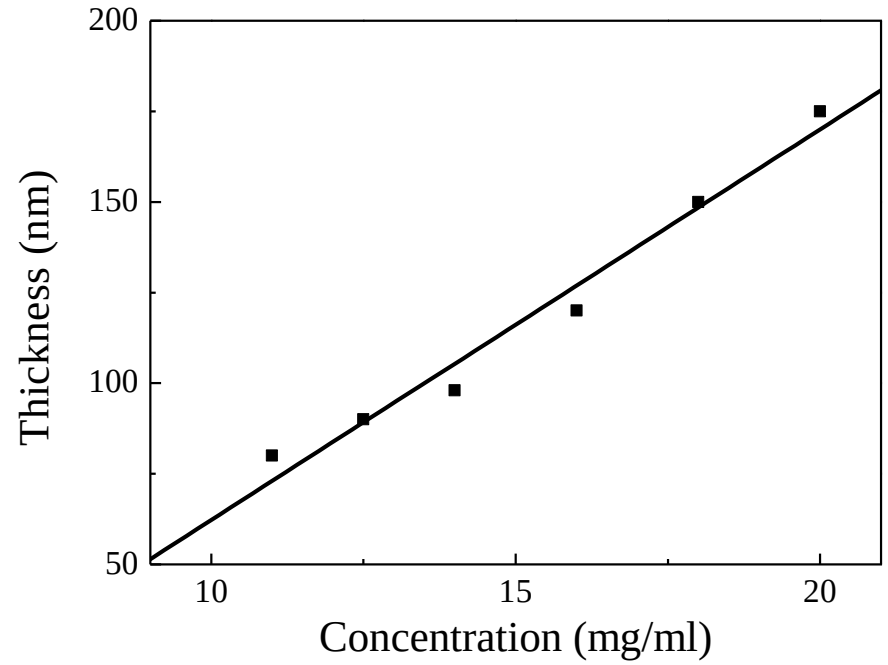

Fig.4.1. Film thickness as a function of solution concentration of PFO; spin-coating condition: 2000 RPM and 5 sec RAMP for 60 sec.

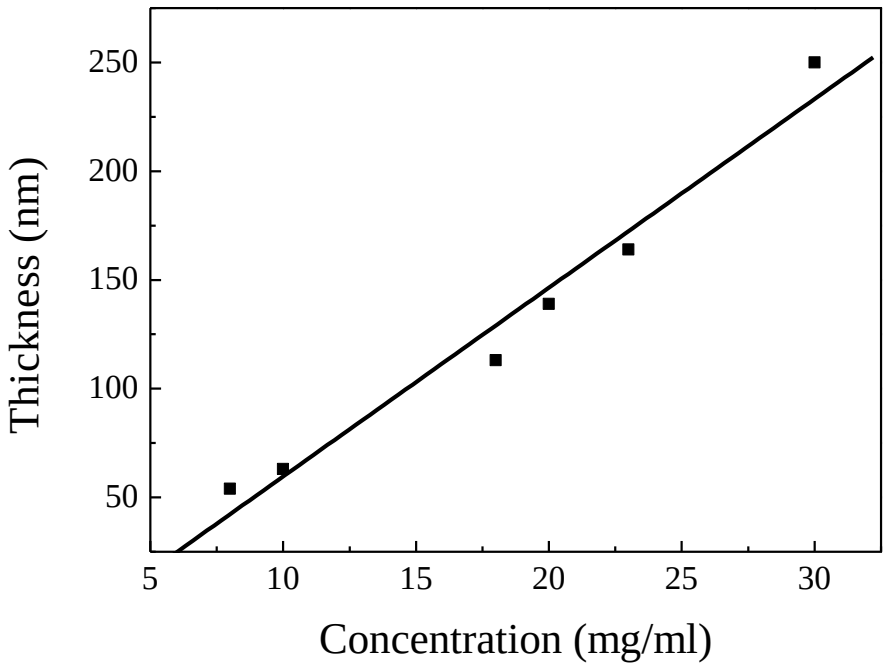

Fig.4.2. Film thickness as a function of solution concentration in F8BT; spin-coating condition: 2000 RPM and 5 sec RAMP for 60 sec.

4.1.2 PL and Absorption

The absorptions of the samples were measured. Since the output intensity of the samples strongly depended on its own absorption, it was important to obtain the absorption characteristics of PFO and F8BT in order to determine the best wavelength region for pumping laser. The thicknesses of the tested samples were 120 nm and 164 nm for PFO and F8BT respectively, and the thicknesses are required to be thicker than 100 nm to obtain relievable results. The polymers were spin-coated on cleaned fused silica substrates. The absorption spectra of two materials were shown in Fig.4.3. The absorption peaks are 218 nm and 380 nm for PFO; while 210 nm, 321 nm and 461 nm for F8BT. Fig.4.3 shows the absorbance of both materials at 355 nm. And it is considered acceptable for energy transfer using the same pumping laser (λ= 355 nm) to the gain mediums without incurring significant loss.

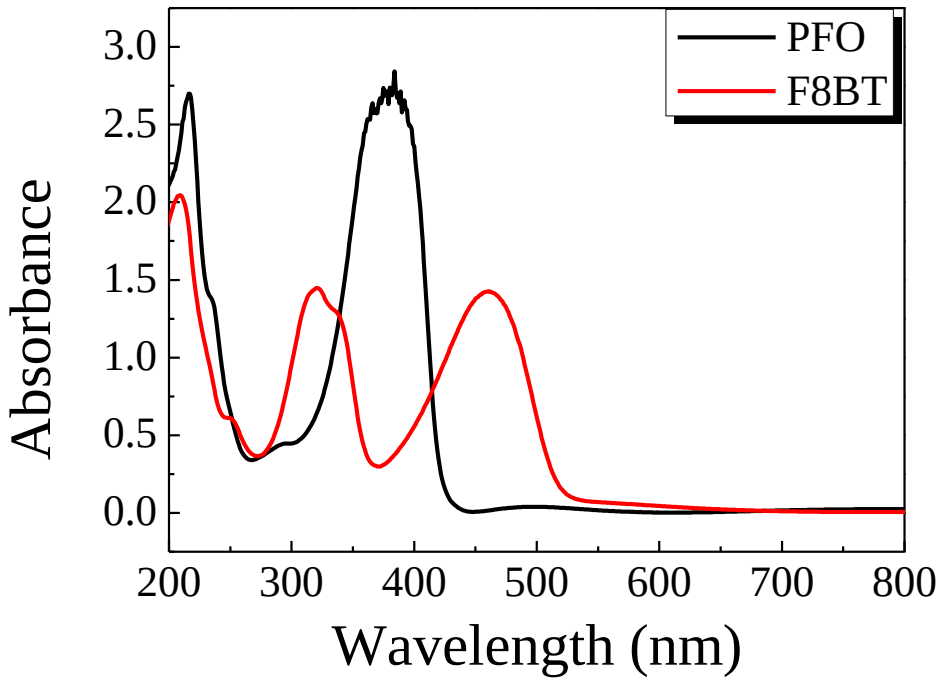

Fig.4.3. Absorption of PFO (120 nm) and F8BT (250 nm) thin films.

Photoluminescence (PL) spectra of PFO and F8BT are shown in Fig.4.4. The fluorescence measurement described in Section 3.4.2 was used to obtain the PL spectra. The PL emission peak of PFO is 423 nm and a shoulder at 429 nm; the peak of F8BT is 545 nm. For the PL of F8BT, it was suspected that the broad emission was indeed due to two emission peaks since the emission spectrum is not symmetric and we will discuss more in Section 4.2. In Fig.4.4, we also observed that both polymers have broad PL spectra and it is possible to tune the lasing emission across a wider visible range [39, 41]. Comparing PL spectra (Fig.4.4) and absorption spectra (Fig.4.3), obvious Stokes' shift is observed. As mentioned in Section 2.3.1, the Stokes' shift is due to the changing of molecule positions. And the Stokes' shift also can enhance the efficiency of emission by decreasing the self-absorption.

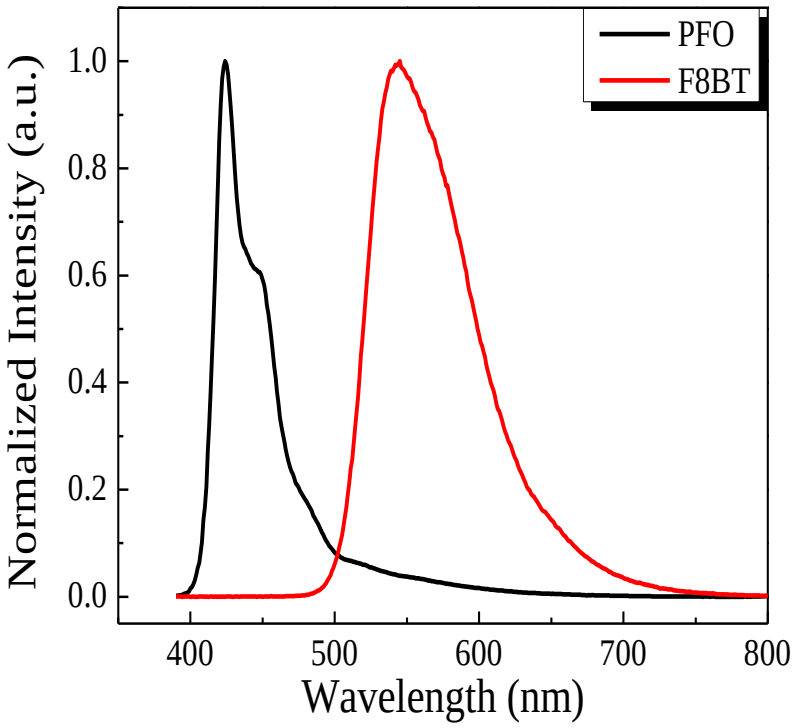

Fig.4.4. Photolunminescence of PFO and F8BT thin films optically pumped by He-Cd laser (λ: 325 nm).

4.2 Amplified spontaneous emission

Amplified spontaneous emission (ASE) is a phenomenon of optically dense in the gain medium. Also, ASE is the primary method to measure gain efficiency of materials and evaluate the possibility of the materials being used in organic laser [41]. In this section, ASE measurement (Section 3.4.3) was used to demonstrate ASE from organic thin films. The third harmonic of Nd:YAG laser was used as the pumping laser (wavelength at 355 nm and 10 Hz). The laser beam was focused and transformed by the concave lens (*f:* -50 mm) and cylindrical lens such that it became a line shape. A slit (5 mm) was added to control the excitation area (A: 5 mm x 300 μm). The excitation area was fixed since the gain is strongly dependent on it. The thicknesses were 120 nm and 164 nm for PFO and F8BT respectively on fused silica substrates, the same as Section 4.1. The samples were excited by pulsed laser light in a strip-shape near the edge of the substrate. The light was waveguided along the length of the excitation area emitting from the edge, and the illustration of experimental setup is shown in Fig.4.5.

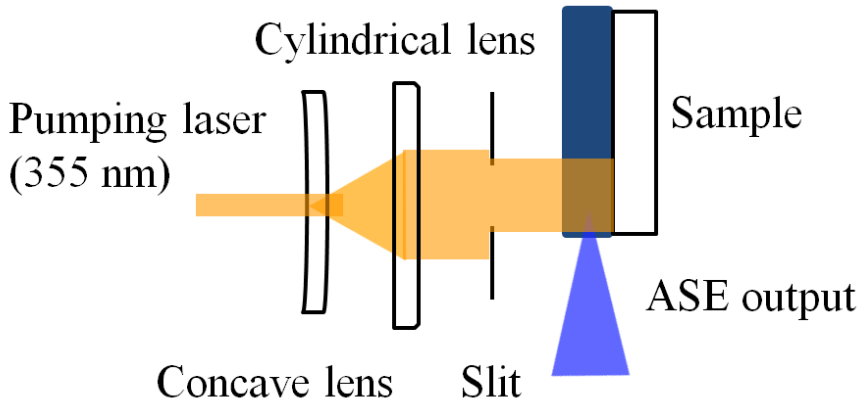

Fig. 4.5 Illustration of experimental setup. The pumping laser (wavelength at 355 nm and 10 Hz) is Nd:YAG laser and laser beam was focused and transformed by the concave lens (*f:* -50 mm) and cylindrical lens. Then laser beam was become a line shape, and added a slit (5 mm) to control the excitation area (A: 5 mm x 300 μm). Finally ASE output was collected from the edge of sample.

During optical pumping, the excitation area of sample was optically dense, and the light was expected to be reflected and propagated repeatedly along the length of the area leading to light amplification. The guided spontaneous emission including the stimulated emission was amplified and emitted from the edge. In order to detect the lasing emission, the convex lens (*f*: 30 mm) and fiber coupled Ocean optics were used. The lasing spectra of PFO and F8BT are shown in Fig.4.6 and Fig.4.7, and the PL spectrum is also included for comparison. With the right gain condition, the amplification of the specific wavelength of light was larger compared to other wavelengths with spectral narrowing. Fig.4.6 and Fig.4.7 show obvious change of spectral shape between PL and ASE. In Fig.4.6, the ASE peak of PFO is 450 nm, which is very close to its shoulder. At optically dense condition, the energy at 450 nm was amplified and the intensity of that wavelength was much higher than the others. Thus, ASE was achieved. Also, a significantly less intense PL shoulder emission peak around 400 nm to 500 nm ranges (less than 0.1 a.u.) was obtained. It may be due to the convex lens collecting fluorescent light. As expected, the ASE signal could be collected from the edge, implying that the light was propagating along the length of the excitation area. Also, the spectrum intensity is wavelength-dependent which can be described by Equation 2.5. For F8BT, similar results were observed. The peak of ASE is 571 nm. In the previous discussion (Section 4.1), it was suspected that the broad PL emission of F8BT may involve two peaks and here (Fig.4.7) the positions of the peaks were confirmed in the ASE spectrum. Comparing the PL shoulder of F8BT and PFO ASE spectra, the PL shoulder of F8BT was relatively higher (Maximum intensity ~0.3 a.u.). This may be caused by the convex lens collecting the fluorescent light and also the pumping laser. The overlap of wavelength of the laser (355 nm) with the absorption peak of F8BT is not large. Thus the energy transfer to F8BT may not be as efficient as PFO. In summary, using these two gain mediums, PFO and

F8BT, ASE was successfully demonstrated. Both materials have potentials to be used as gain medium for organic semiconducting laser.

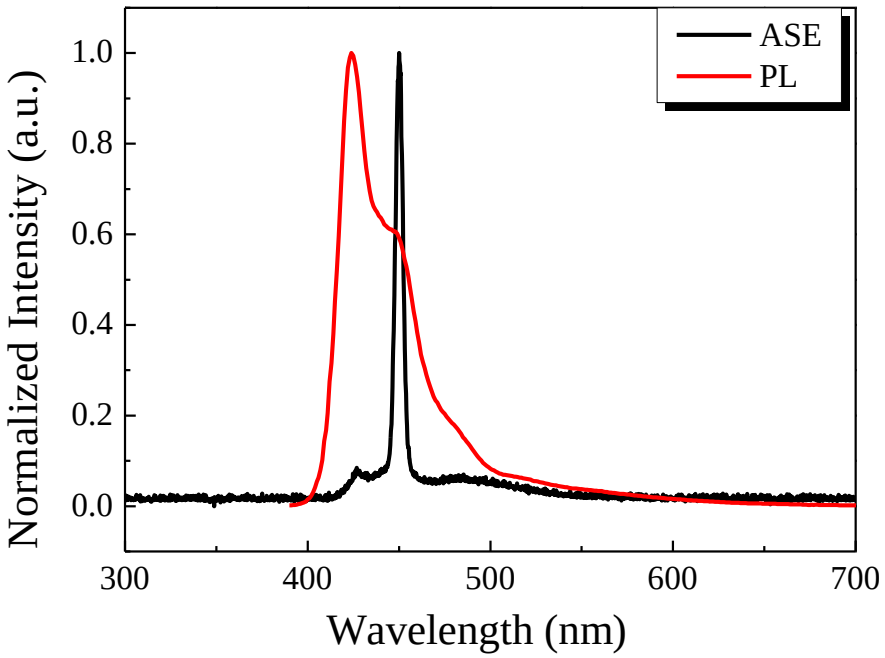

Fig.4.6 ASE and PL spectra of PFO (120 nm); The samples were pumped by Nd:YAG laser (355 nm, 10 Hz) and the excitation area is 5 mm x 300 μm; and the ASE output is collected from the edge of the sample by the fiber coupled spectrometer.

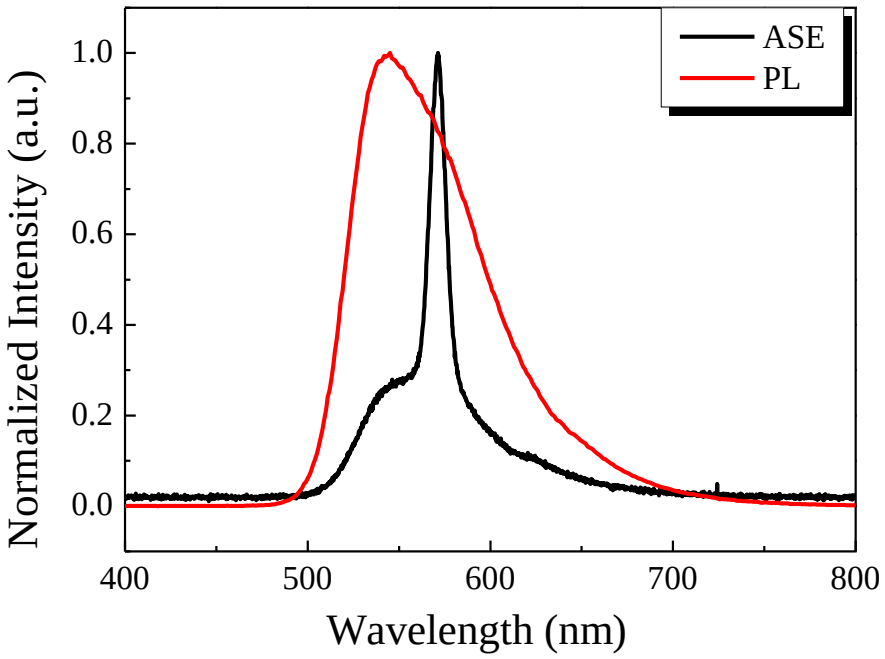

Fig.4.7 ASE and PL spectra of F8BT (164 nm); The samples were pumped by Nd:YAG laser (355 nm, 10 Hz) and the excitation area is 5 mm x 300 μm; and the ASE output is collected from the edge of the sample by the fiber coupled spectrometer.

4.3 Energy dependence

Spectral narrowing is one of the clues indicating that there is a gain of the material during optical pumping. Besides that, a considerable increase in the output intensity can be observed when the gain medium is optically pumped with varied energy density. Using the efficiency measurement, the energy dependence of the tested samples was measured. In this section, the full width half maximum (FWHM) and the output intensity as a function of pumping energy were presented to demonstrate existence of the gain leading to ASE. The structure and thickness of the tested samples are the same in Section 4.2.

4.3.1 FWHM as function of pumping energy

FWHM represents the width of the spectrum in half of the total intensity

(Fig.4.8), which can indicate that the spectrum is changing from PL to ASE and show the gain medium having a net gain.

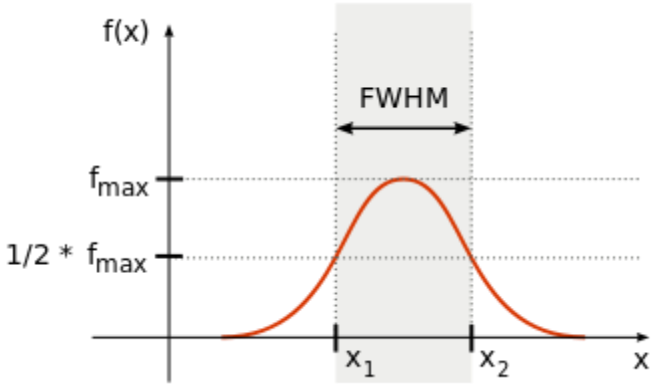

Fig.4.8 Schematic definition of FWHM

By investigating the change in FWHM as a function of pumping energy, spectral narrowing could be observed when the pumping energy was above the threshold. Typically, the FWHM of ASE is in the range from 4 to 15 nm depending on different materials and pumping source [41, 83]. The spectral narrowing from PFO and F8BT samples can be observed in Fig.4.9 and Fig.4.10. For PFO, the FWHM is around 43 nm under low pumping energy density (<80μJ/cm^2). By increasing the pumping energy density (>80μJ/cm^2), the FWHM dramatically drops to 5 nm, implying spectral narrowing and the existence of net gain. And F8BT exhibited similar properties as PFO (Fig.4.10) and the FWHM reduces from 66 nm to 15 nm with increased pumping energy density.

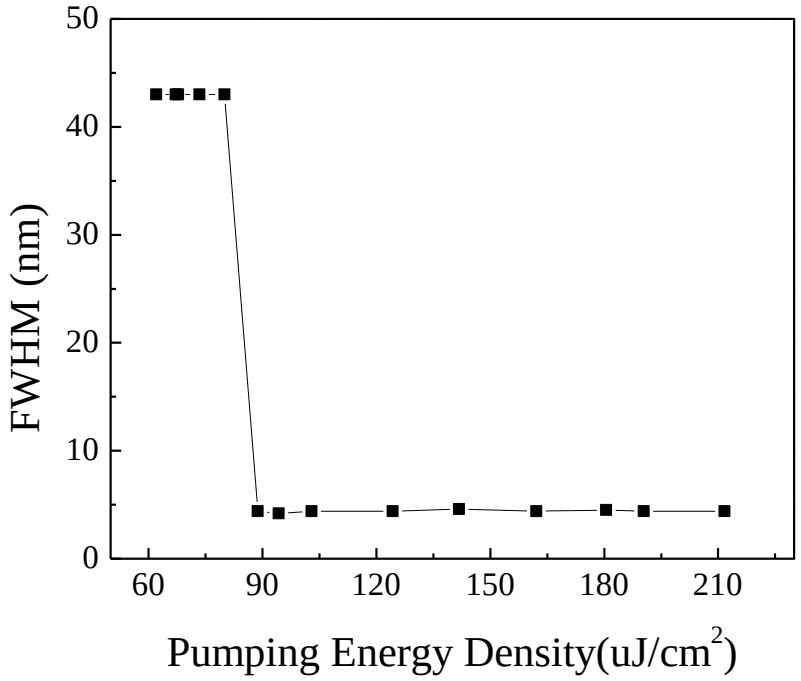

Fig.4.9 FWHM as a function of pumping energy density of PFO

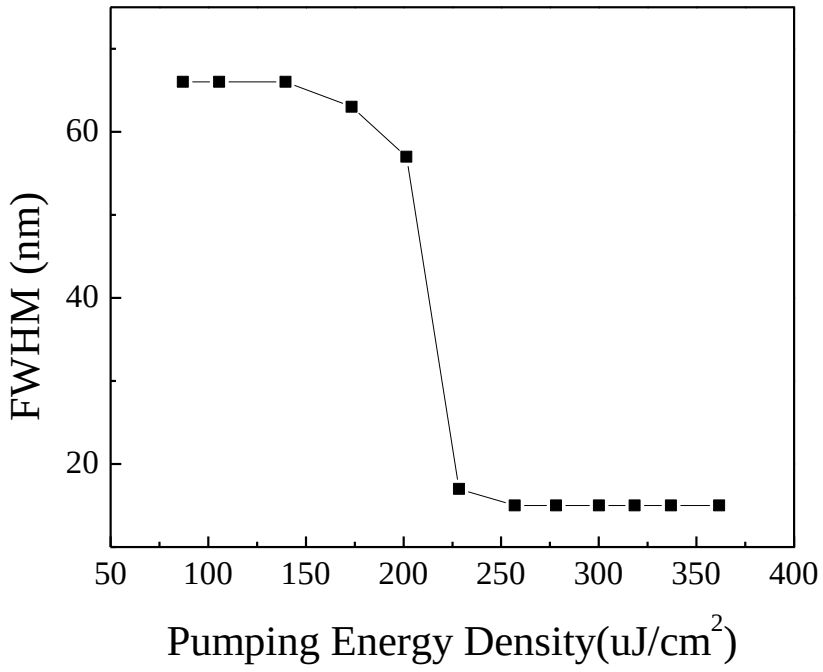

Fig.4.10 FWHM as a function of pumping energy density of F8BT

4.3.2 Output intensity as a function of pumping energy

The output intensity is strongly dependent on the pumping intensity. Threshold is one of essential parameters in lasing. In lasing, an obvious threshold in both the output power and line width can be determined [36]. Threshold can be determined by observing a point that the slope is changed dramatically at specific pumping intensity. At that pumping intensity, a surge in output intensity, a sudden reduction in FWHM can be observed. As shown in Fig.4.11, the output intensity increases slowing at low pumping energy density below the threshold. When the energy density is above the threshold, the output intensity suddenly increases with a more inclined slope. By using log scale for energy density and intensity to process the data, the threshold can be easily determined at change in gradient point of the slope. The threshold of 120 nm PFO is 130 $\mu J/cm^2$ (Fig.4.11) while that of F8BT is 139 $\mu J/cm^2$(Fig.4.12). To conclude, by analyzing the energy dependence of FWHM and output intensity as a function of pumping energy, spectral narrowing and threshold were identified in both PFO and F8BT neat films. It further supports that these samples were in net gain condition and exhibited ASE. The thresholds which are determined from Section 4.3.1 are slightly lower than the thresholds which are determined in this section. The reason is that the definitions of threshold are different: one is determine at the FWHM drops by half, one is determine at the ASE output intensity change. And the change of slope in energy dependence takes place when the spectrum is already narrow. Also, for F8BT, the ASE spectrum (showed in Fig. 4.7) showed relatively high intensity of the shoulder that makes a proper determination of the FWHM difficult.

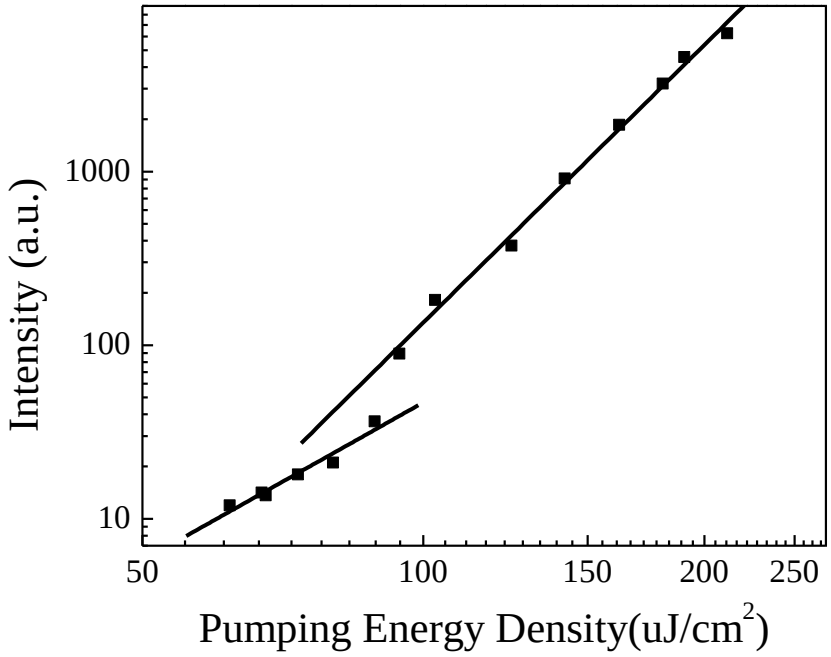

Fig.4.11 Output intensity as a function of pumping energy density of PFO; showing the clear threshold at 130 μJ/cm^2.

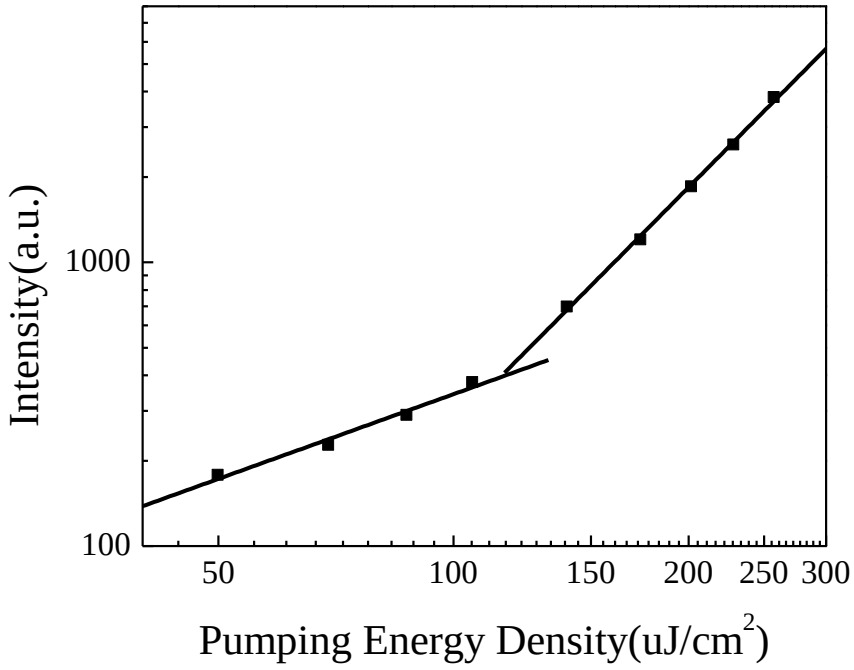

Fig.4.12 Output intensity as a function of pumping energy density of F8BT; showing the clear threshold at 139 μJ/cm^2.

4.4 Cascaded organic thin films

In this section, a device consisting of two cascaded organic thin films was described. The tunability of the color of emission light due to ASE from the device was demonstrated. Also, the angle-dependent of ASE was investigated.

4.4.1 Fabrication of cascaded organic thin films

PFO and F8BT are both efficient light emitting polymers (Section 4.2). In fact, it is possible to combine the emission colors of PFO and F8BT (blue and green) to give white light. In this part of the work, PFO and F8BT were dissolved in toluene solution with a concentration of 16 mg/mL and 23 mg/mL respectively, and then deposited on cleaned fused silica substrates by spin-coating with the same conditions in Section 3.3.1. The thickness of PFO and F8BT films were 120 nm and 250 nm respectively. As shown in Fig. 4.13 (a), the cascaded thin film system includes PFO and F8BT bounded together by 60 μm optically clear adhesive (OCA) [84]. The OCA is designed to separate the two layers completely to prevent any mixing. Without the OCA, they could mix into each other because same kind of solvent was used in the dilution of the polymers. The refractive index of OCA is around 1.48, which is smaller than that of PFO and F8BT [85]. The lower refractive index of OCA provides a better condition for the device; as the active layer can have higher chance for total reflection and thus enhancing the intensity of ASE.

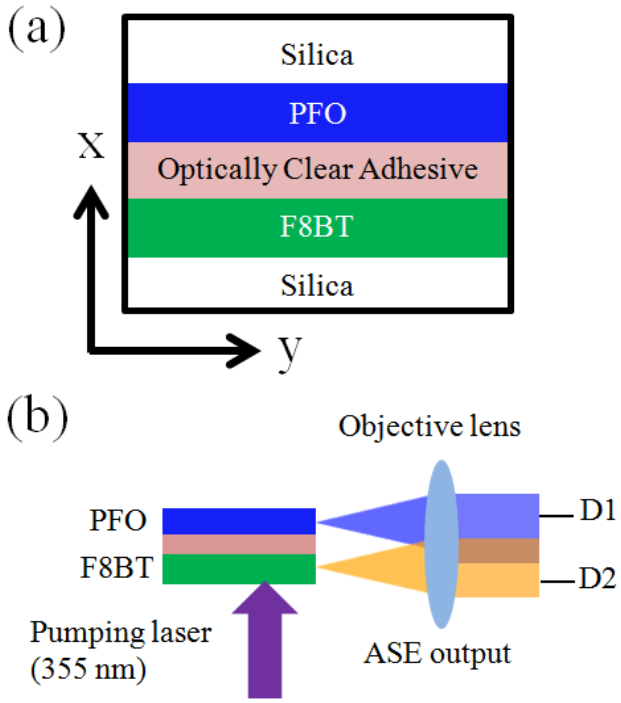

Fig.4.13 (a) Cross-section of cascaded films with fused silica (1 mm), PFO (120 nm), optically clear adhesive (60 μm), F8BT (250 nm), and fused silica (1 mm); (b) ASE measurement configuration. The cascaded films is pumped with Nd:YAG laser (355 nm, 10 Hz) and the excitation area is 5 mm x 300 μm; and ASE output is collected from the edge of the sample by the fiber coupled spectrometer.

In ASE experiment (Fig.4.13 (b)), the PFO/F8BT cascaded films were pumped by third harmonic generation of Nd:YAG laser at wavelength λ of 355 nm with repetition rate of 10 Hz and pulse width of 5 ns. The laser beam was first diverged by a concave lens (f: 50 mm), and then squeezed into stripe beam by a cylindrical lens. Finally, the stripe beam was focused on to the device after eliminating the non-uniform edges of the stripe laser spot by adjustable slits (5 mm). The area size of the rectangular laser spot is 5 mm x 300 μm. The spontaneous emission and ASE signals from PFO and F8BT were collected at the edge of the device using the objective lens (f: 30 mm) and analyzed by fiber coupled spectrometer (Ocean Optics, USB 4000). In Fig. 4.13(b), D1 and D2 represents the highest intensity positions of

PFO and F8BT respectively. The highest intensity positions were confirmed using the peak wavelengths showing in Section 4.2 (450 nm and 575 nm). In addition, a photo diode was used to monitor and calibrate the pumping energy of the laser.

The structure of the device was fused silica substrate/ F8BT/ OCA/ PFO/ fused silica. The pumping laser passed through the F8BT-side first because it has lower absorption at 355 nm. The sample could be tuned from emitting blue, white to green light from the same device by changing the position of the receiving fiber. This design and method used here also has a potential in designing the different emission spectra of organic light emitting devices, or even tunable color of light source.

4.4.2 Properties of cascaded organic thin films

Fig.4.14 shows the transmission efficiency of optical clear adhesive, PFO, F8BT and PFO/OCA/F8BT cascaded films. It shows the OCA has a high transmittance for the whole visible range, suggesting low optically loss. For the cascaded films (open circles) near UV-region, there are two corresponding absorption peaks at ~350 and 450 nm arisen from PFO and F8BT absorption respectively. Apart from induced absorption of the materials, the transmittance is more than 70%, which is considered acceptable for optical pumping.

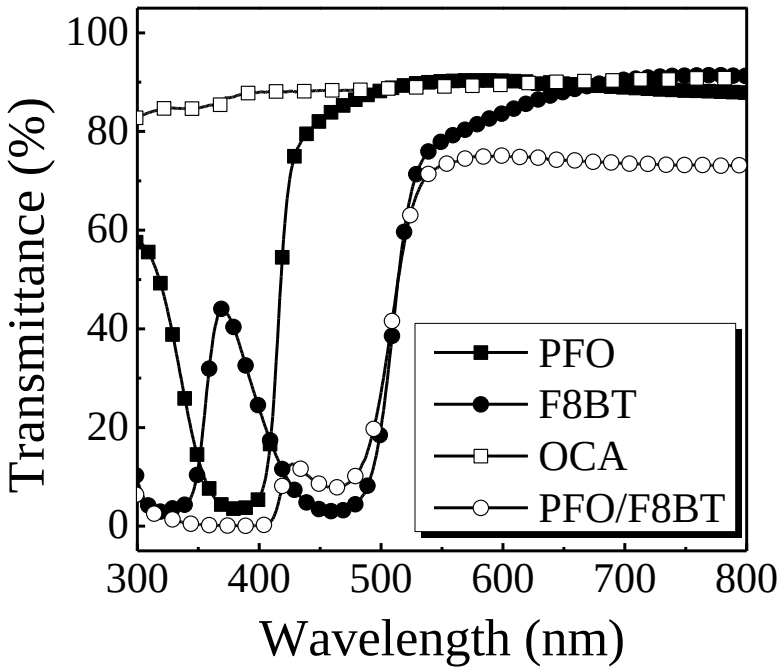

Fig.4.14 Transmittance of (i) PFO (120 nm, filled squares), (ii) F8BT (250 nm, filled circles), (iii) Optically Clear Adhesive (60μm, open squares) and (iv) Cascaded PFO (120 nm)/F8BT (250 nm) films (open circles).

4.4.3 ASE spectra

In ASE experiment, the Nd:YAG laser beam was incident at normal direction of the sample. The ASE signals from PFO (ASE_{PFO}) and F8BT (ASE_{F8BT}) were separated in the near field by the OCA, and the two directional emissions were then imaged into the far field using an objective lens and a convex lens with focal length of 30 mm. The spatial overlaps of ASE_{PFO} and ASE_{F8BT} at the detection point are determined by the imaging system. The scanning of the signal was along the x-direction. Fig. 4.15 is the normalized ASE spectra at different positions of the edge of the sample with the same pumping energy density at 247 μJ /cm^2. D1 and D2 were defined in Fig.4.13 (b), the white light with Commsion Internationale d'Eclairage (CIE) coordinates (0.32, 0.35) is the white light ASE. The ASE spectra strongly depended on the spatial distribution of the two overlapped emission beams. The ASE_{PFO} (peak position: 450

nm) was dominant at position D1 while ASE_{F8BT} (peak position: 575 nm) was dominant at D2. Two ASE intensities showed an inverse proportion to each other during the scanning process.

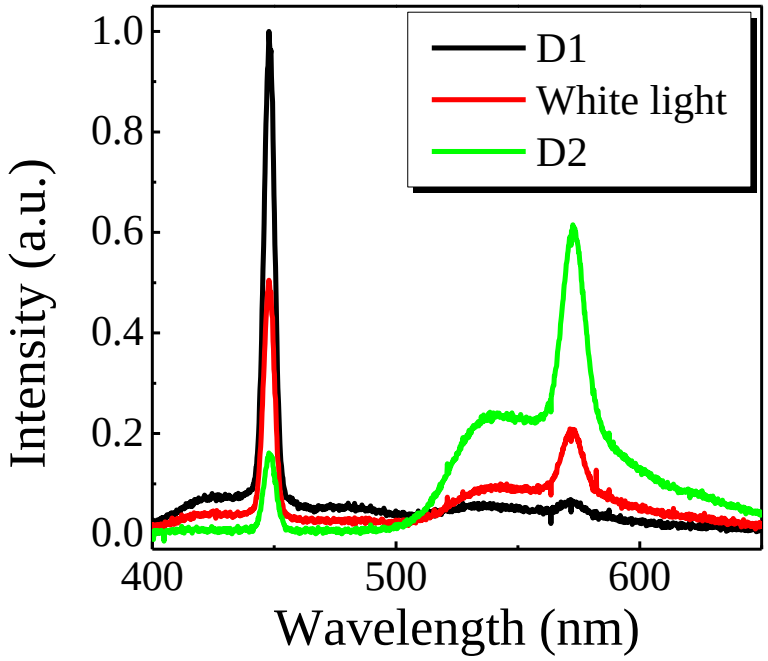

Fig.4.15 Normalized ASE spectra in different positions

(pumping energy density: 247 μJ/cm^2)

The color of output ASE would change when the collection fiber moved from D1 to D2. Equation 4.1 can be used to calculate the CIE coordinates [10] in color space based on the measured spectra (Fig. 4.16).

$$X = \int_{380nm}^{780nm} PL(\lambda) \bullet \bar{x}(\lambda) \bullet d\lambda \qquad CIEx = \frac{X}{X+Y+Z}$$

$$Y = \int_{380nm}^{780nm} PL(\lambda) \bullet \bar{y}(\lambda) \bullet d\lambda \qquad CIEy = \frac{Y}{X+Y+Z} \qquad (4.1)$$

$$Z = \int_{380nm}^{780nm} PL(\lambda) \bullet \bar{z}(\lambda) \bullet d\lambda \qquad CIEz = \frac{Z}{X+Y+Z}$$

where $\bar{x}, \bar{y}, \bar{z}$ *are color matching functions.*

The circle symbols represent the CIE coordinates of the measured spectra. The CIE coordinates can be tuned from (0.42, 0.55) to (0.18, 0.11) with a linear relation. The synthesized white color of the ASE corresponded to CIE coordinates at (0.32, 0.35), which was very close to the center of CIE coordinates (0.33, 0.33) representing white light emission.

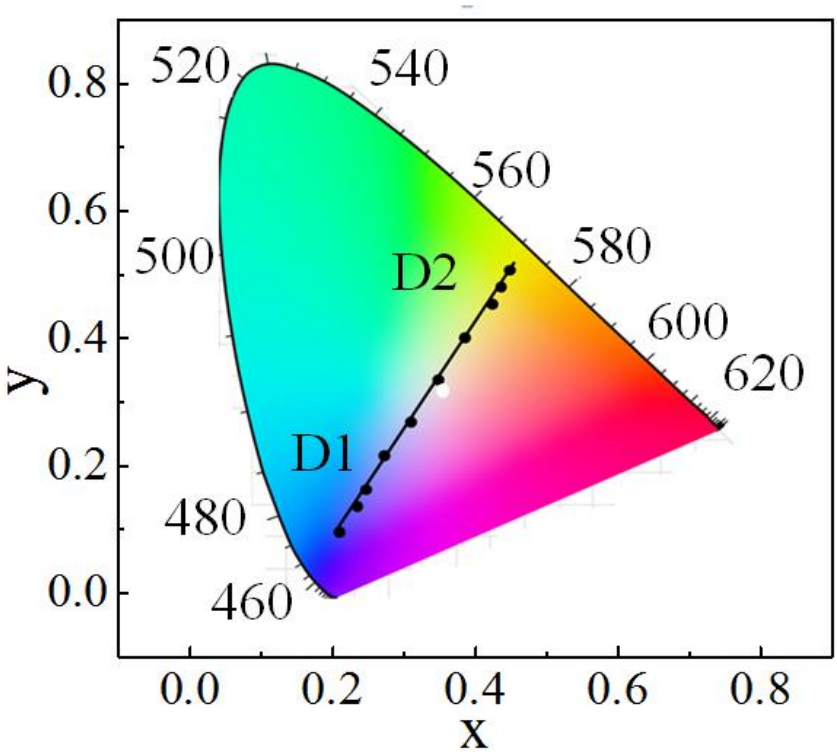

Fig.4.16 The color coordinates (black circle symbols) mapping onto the CIE chart and the center of CIE (0.33,0.33, white circle symbols); showed the linear relationship of CIE shifting calculated from the spectra in different positions; and D1, D2 also located in CIE chart.

4.4.4 Energy dependence

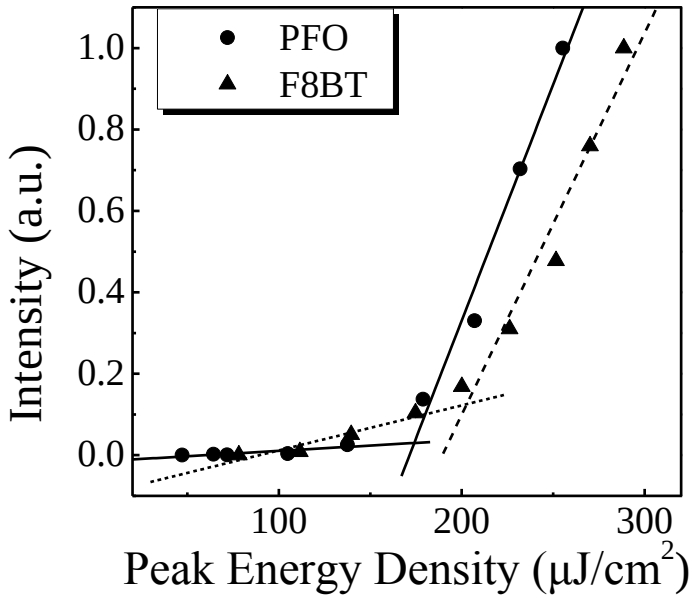

Fig.4.17 Energy dependence of PFO (circles) and F8BT (triangles), and symbols represent the peak value of the ASE spectra under various energy density; showing the clear threshold at 174 μJ/cm^2 and 203 μJ/cm^2 respectively.

Fig.4.17 shows the energy dependence of ASE at maximum intensity, corresponding to the ASE from PFO and F8BT respectively in cascaded films. Below the threshold, the spontaneous emission in PFO and F8BT are dominant. By increasing the pumping energy above threshold, the emission spectra exhibited ASE with thresholds 174 μJ /cm^2 for PFO and 203 μJ /cm^2 for F8BT. Comparing the results in Section 4.2, the single layer of PFO and F8BT had relatively lower threshold (130 μJ /cm^2 and 139 μJ /cm^2). It is mainly due to the absorption of the device itself including the two active layers and the scattering loss due to roughness at each interface. As shown in Fig.4.13 the overall transmittance of the cascaded device is around 75% excluding the transmittance dips due to the active materials), the efficiency of the pumping laser reaching the active layers were dropped. Thus the threshold was larger for the device.

4.4.5 Angle dependent of tunable color emission

The cascaded thin films device in this work demonstrated tunable emission color in far field, At the same time, the device was also sensitive to the distance from the fiber coupled spectrometer in x and y directions. To further investigate this effect, a moveable detector was used in the measurement setup (Fig.4.18). The lasing emission first passed through an objective lens (10x), and was focused by the focus lens (*f*: 30 mm), then collected by the fiber coupled moveable spectrometer. It was moved along the x and y direction for detecting output intensity.

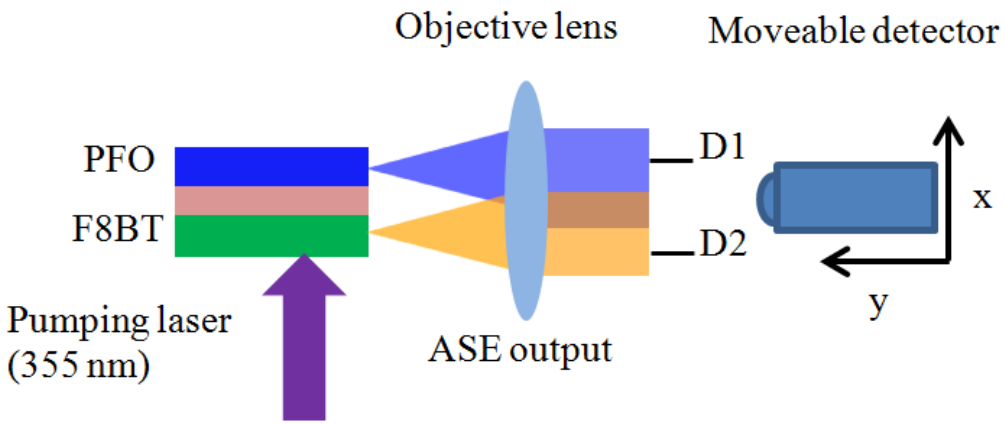

Fig.4.18 Illustration of experimental setup with the moveable fiber coupled spectrometer.

4.4.5.1 x-direction

As mentioned in Section 4.4.3, the intensities of ASE_{PFO} and ASE_{F8BT} had an inverse proportional relating in the x-direction. The peak intensity ratios between PFO and F8BT were used to evaluate the change of the distance along x-direction. The intensity ratio was obtained by dividing the peak intensity of PFO by that of F8BT (Fig.4.19). The distance was calculated for lens correction. The effective range is 147± 7.3 μm from 26 μm to173 μm in distance. The effective range is the distinguishable intensity between PFO and F8BT ratio, and the resolution is 15 μm.

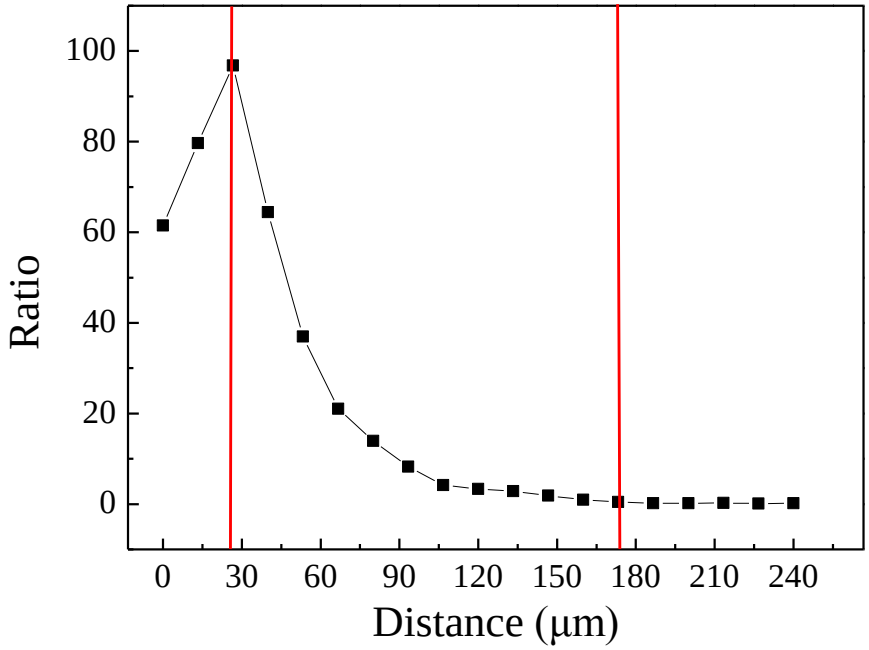

Fig.4.19 The ratio (the peak intensity of PFO/the peak intensity of F8BT) as a function of distance having effective range: 147 μm (from 26 μm to 173 μm, bewteen the red straight line).

4.4.5.2 y-direction

For y-direction, original ASE_{PFO} and ASE_{F8BT} peak intensities were used but not the ratio as a parameter for the conversion to distance. It is because in this direction the peak intensities both decreased as the distance increased. Thus, the ratio between the intensities remained the same, and it was no longer effective for the evaluation. Besides, the lens correction was not needed, as the size of lasing spot was not affected. Fig.4.20 shows the PFO and F8BT intensities as a function of distance along the y-direction. It shows that the effective range was 60 mm from 6 mm to 66 mm. After calculation, the accuracy is ±3.8 mm and the defined resolution is 8 mm. In y-direction, both ASE peak in the lasing spectra was decreased when the detector was moved away from the sample (Fig.4.21).

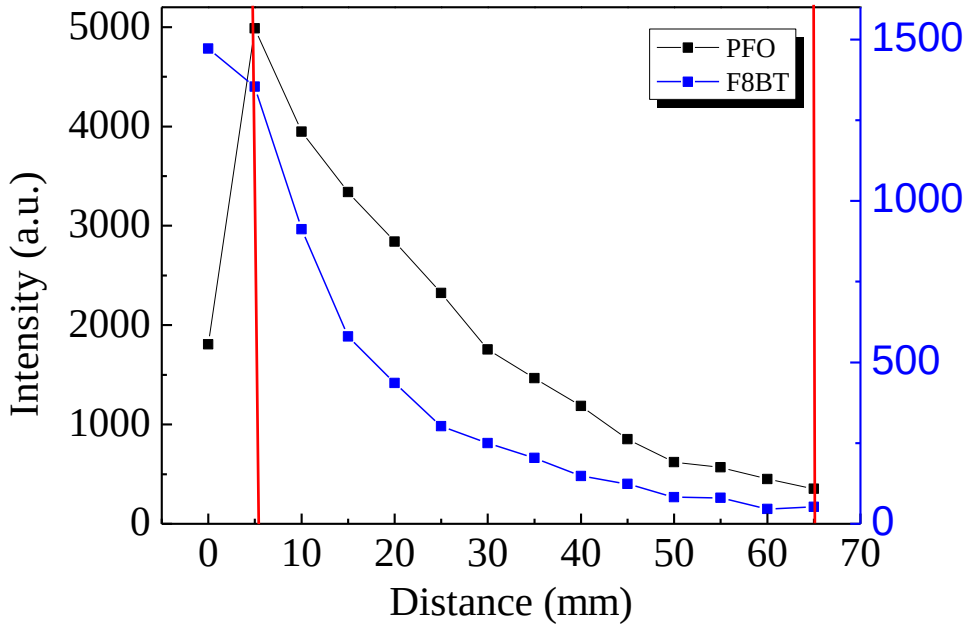

Fig.4.20 The peak intensity of PFO and F8BT as a function of distance having the effective range: 60 mm (from 6 mm to 60 mm, bewteen the red straight line).

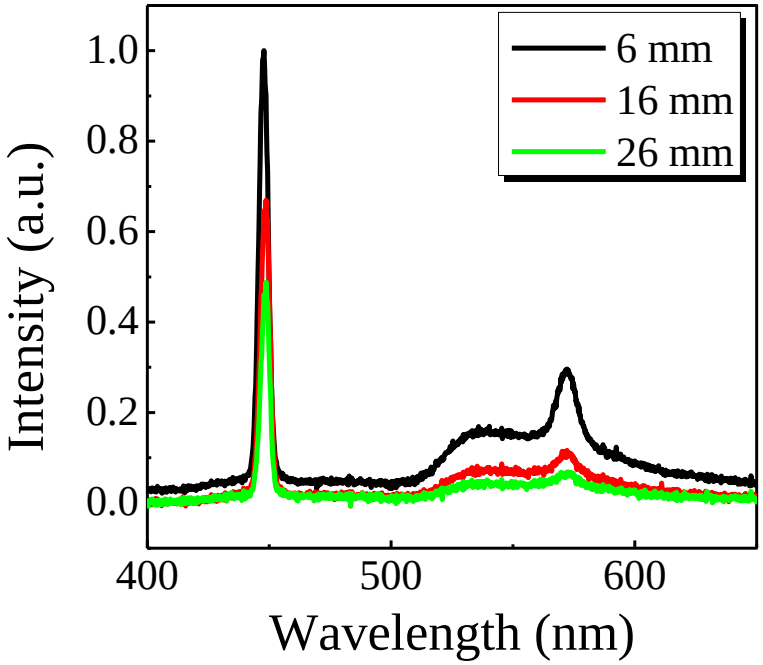

Fig.4.21 Normalized ASE spectra in different position along Y direction (pumping energy density: 247 μJ/cm^2)

These results demonstrated a device made of cascaded organic thin films. The

ASE from the two materials, PFO and F8BT, can be obtained simultaneously when optically pumped by solid state laser. ASE was achieved in the far field of the device with tunable color. And in the study of the relationship between measurement position and distance in both x- and y-directions in terms of ASE peak intensity; this device could be used for distance measurement and vibration detection of distance measurement.

CHAPTER 5 DISTRIBUTED FEEDBACK LASER

Distributed feedback (DFB) structure is a common technique in organic semiconducting lasers [24-25, 64, 66-67]. DFB structure was first employed by containing the organic dyes and using inorganic laser design [62, 86]. In this section, we used three 2D grating having different periods (270 nm, 290 nm, and 310 nm) as the DFB structure. The gratings were designed by us and fabricated by commercial company on 1 mm fused silica substrate covering an area of 1.5 mm x 1.5 mm. With the DFB structure, the threshold was reduced and the wavelength of the lasing emission could be controlled effectively.

5.1 Simulation of DFB structure

The simulation was carried out using finite-difference time-domain (FDTD) numerical analysis software [87] to evaluate the transmittance of the samples in order to identify the Bragg wavelength. DFB lasers were made by spin-coating 134 nm thin films of PFO on the grating substrate. The grating depth is about 50 nm. The structure of the sample for FDTD simulation is shown in Fig.5.1. The parameter in the simulation was the period of gratings (270 nm, 290 nm, and 310 nm). In the modeling, a Gaussian incident light beam with wavelength 355 nm was directed from the top of the sample. The monitor was designed to locate at the bottom of the sample to obtain transmittance and electric field strength.

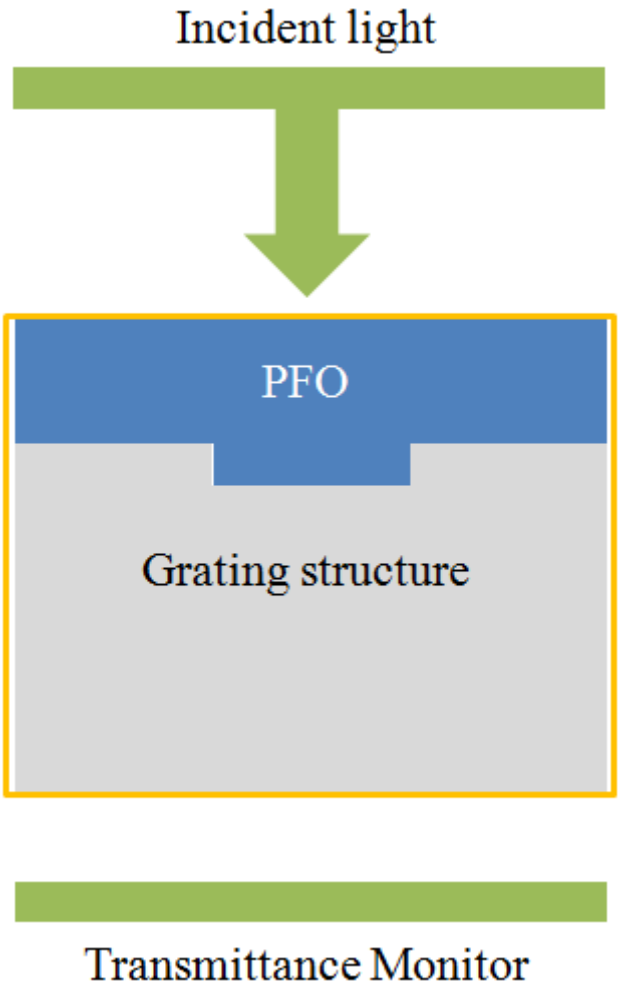

Fig.5.1 The design of DFB structure in FDTD; showing the incident light on the top of the sample, also using transmittance monitor to simulate the results.

The lasing wavelength is related to Bragg wavelength, and Bragg wavelength can be calculated using Equation 2.6. The calculated Bragg wavelength of the gratings were around 450 nm, taking 1.7 and 1.5 as the refractive index of the organic polymer and the substrate respectively, and the order of diffraction is 2. As the lasing efficiency is strongly dependent on the overlapping between Bragg wavelength and emission of the gain medium, PFO was used as the gain medium in this experiment, since the calculated Bragg wavelength is within PFO emission (Fig. 4.4). Bragg wavelength was observed in the transmittance graph obtained by simulation (Fig.5.2). The overall transmittance in visible range is ~70%, and the drop near 420 nm was due

to PFO absorption. In Fig.5.2, observable transmission dips located at 430 nm, 446 nm and 467 nm. These peaks represent the positions of lasing mode and Bragg wavelength. The result was consistent with the calculated Bragg wavelength using Equation 2.6.

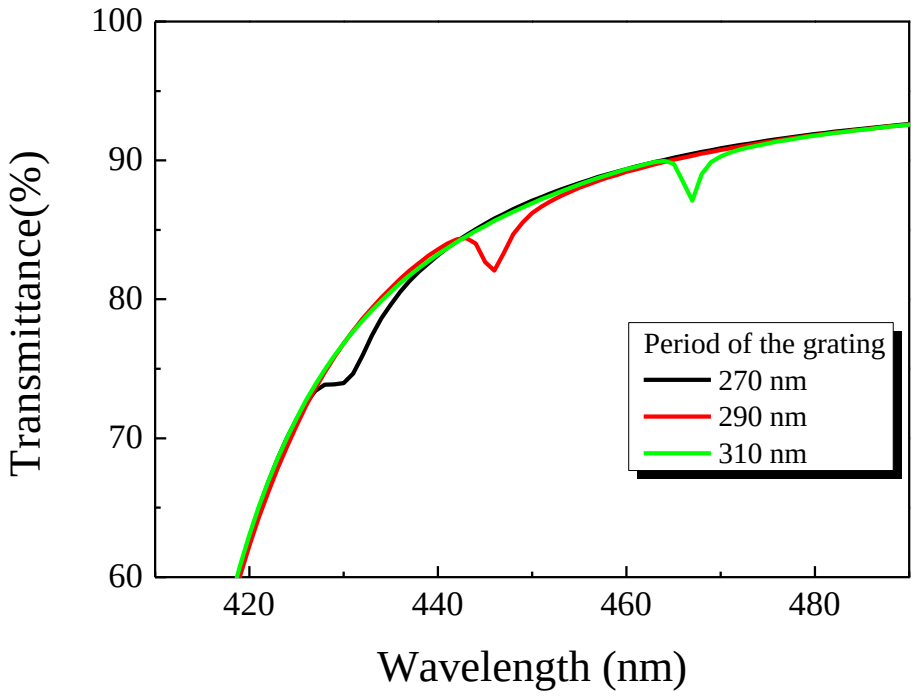

Fig.5.2 Calculated transmittance of DFB laser with grating period 270 nm, 290 nm and 310 nm.

The mode profile of those samples were also simulated (Fig.5.3). It is confirmed that only one optical mode occurred inside the active layer. However, the result with 310 nm of grating period is different from the others. Fig.5.3 (c) shows less intensity contrast between the centre of emission and the peripheral region suggesting that the DFB laser (310 nm) may not be efficient, in fact the intensity of the emission was closer to that of PL intensity.

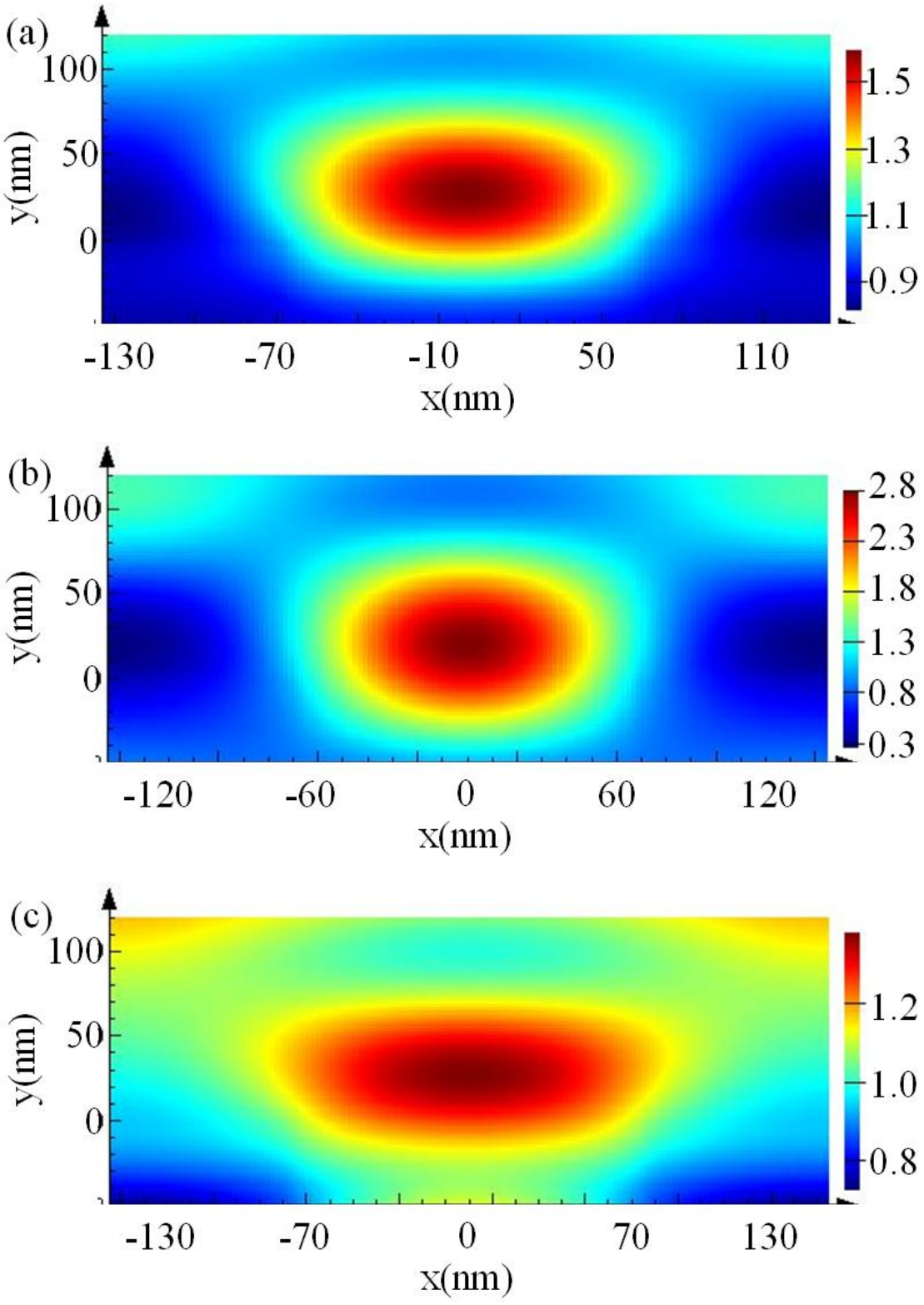

Fig.5.3 Calculated mode profile of DFB laser (a)with 270 nm periods; (b)290 nm periods; (c)310 nm periods.

SEM images of grating structures are shown in Fig.5.4, where the 2-D gratings and their periods are confirmed.

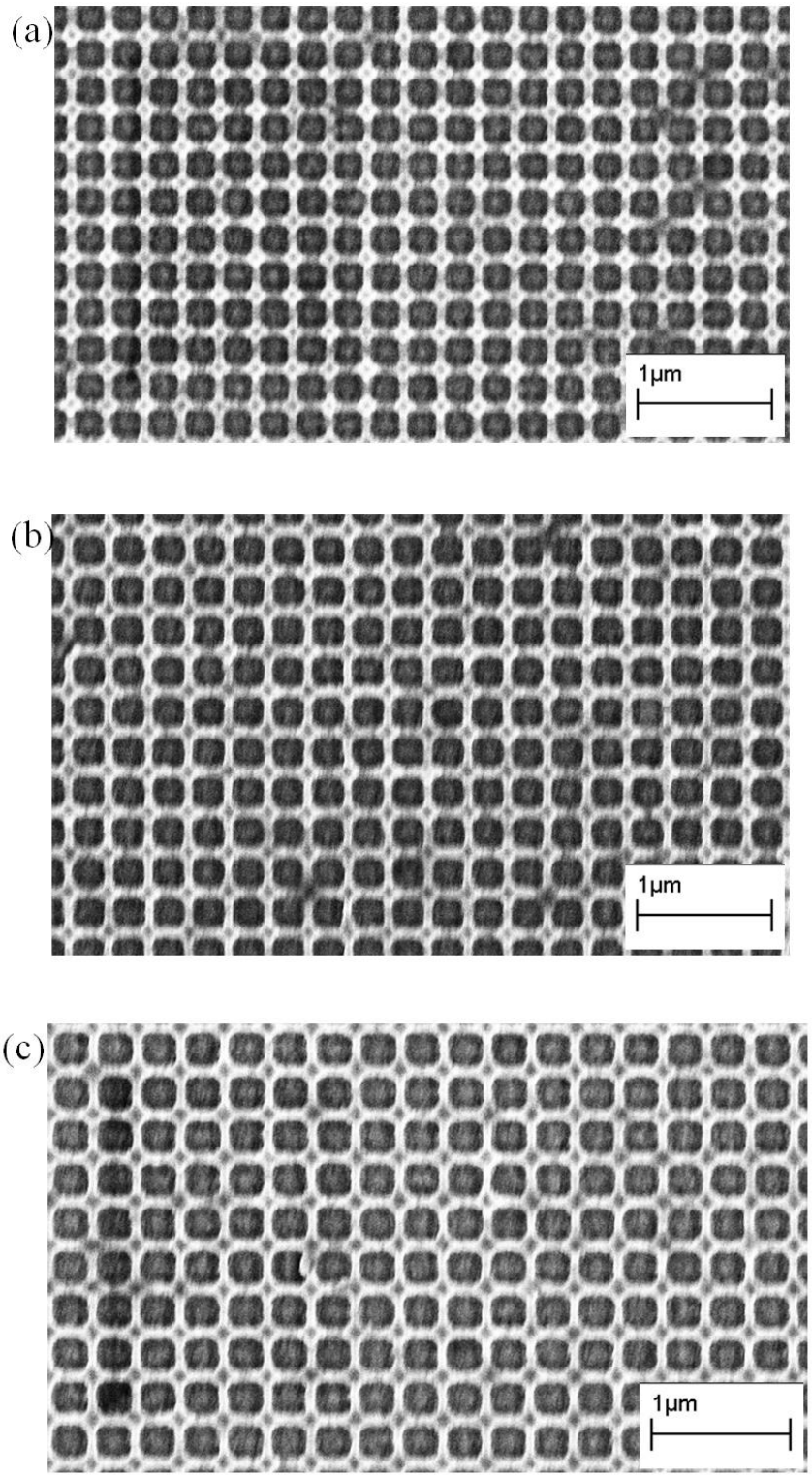

Fig.5.4 SEM images of 2-D grating patterns, (a)with 270 nm periods; (b)290 nm periods; (c)310 nm periods.

5.2 Laser spectra

DFB structure draws much attention because it can provide long gain lengths, high optical confinement of waveguide mode and modulation of emission peak, leading to lower threshold and opening possibility for electrical pumping [20]. Fig.5.5 shows the normalized laser emission spectra of the three samples, with devices structure of fused silica substrate/ gratings (periods: 270 nm, 290 nm, and 310nm)/ PFO (134 nm). Each sample was optically pumped with the same energy density 120 $\mu J/cm^2$. As mentioned in Section 2.4.2, DFB lasers are able to manipulate the output emission in vertical direction, thus the position of the receiving optical fiber was moved to the back of samples for measurement. Among the distinct periodic corrugation, the significant change of laser emission was observed. The peaks of laser spectra are 441 nm, 457 nm, and 478 nm for grating period 270 nm, 290 nm, and 310 nm respectively. The experimental laser emission peaks are consistent with the calculated transmittance peaks (Fig5.2 and Fig. 5.5). Owing to the influence of DFB structure, the laser emissions were controlled at specific wavelengths. Spectral narrowing is also observed. The FWHM of the three DFB lasers is 1.5 nm which was slightly higher than other semiconductor diode lasers [20]. Comparing to the ASE spectrum of PFO neat film (Fig.4.7), the FWHM of the devices using DFB structure is further narrowed. To quantify of the DFB laser, quality factor (Q-factor) can be introduced, which is:

$$Q = \frac{\lambda_o}{\Delta\lambda} \quad [4.1]$$

, where λ_0 is the peak emission wavelength from DFB laser, and $\Delta\lambda$ is the FWHM of the laser spectra. The calculated Q-factor was around 300, which is comparable to conventional lasers [20, 48, 51].

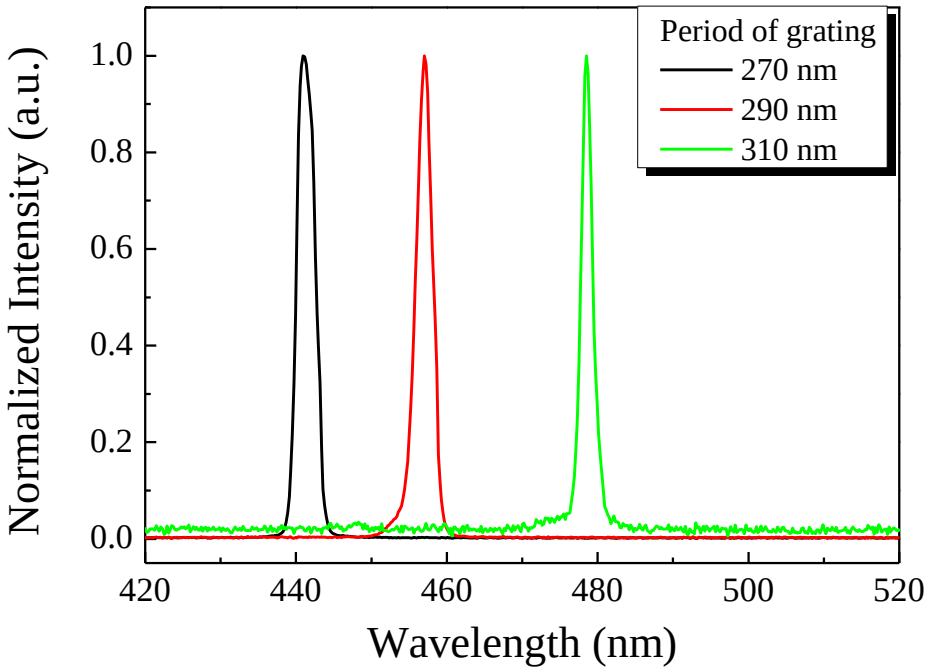

Fig.5.5 Noramlized laser emission spectra from DFB with grating period 270 nm, 290 nm and 310 nm.

5.3 Energy dependence of DFB laser

Energy dependence of DFB laser was also investigated. Efficiency measurement (Section 3.5.1) was used to determine the threshold energy.

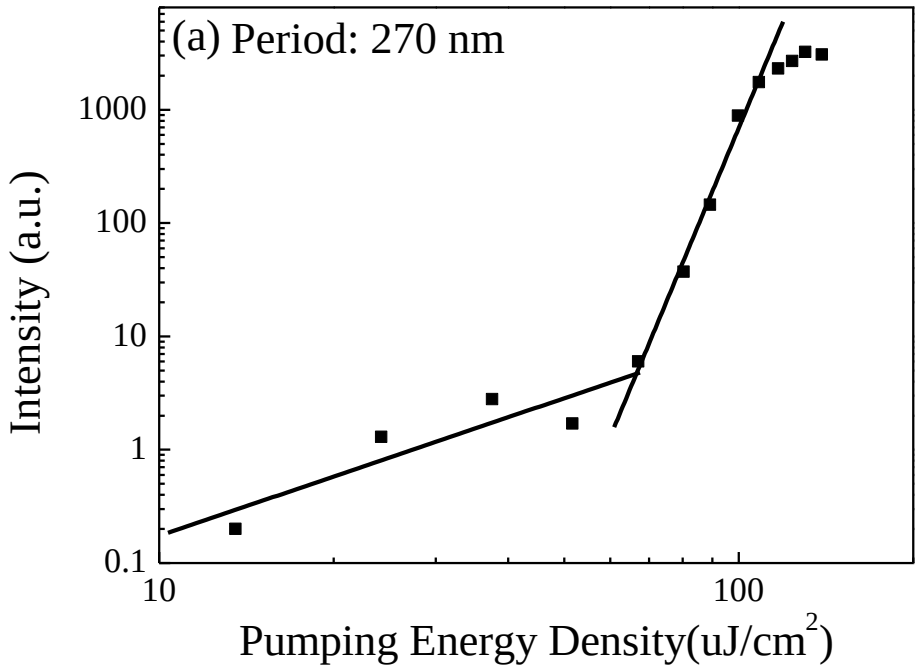
(a) Period: 270 nm
Intensity (a.u.)
1000
100
10
1
0.1
10
100
Pumping Energy Density(uJ/cm2)

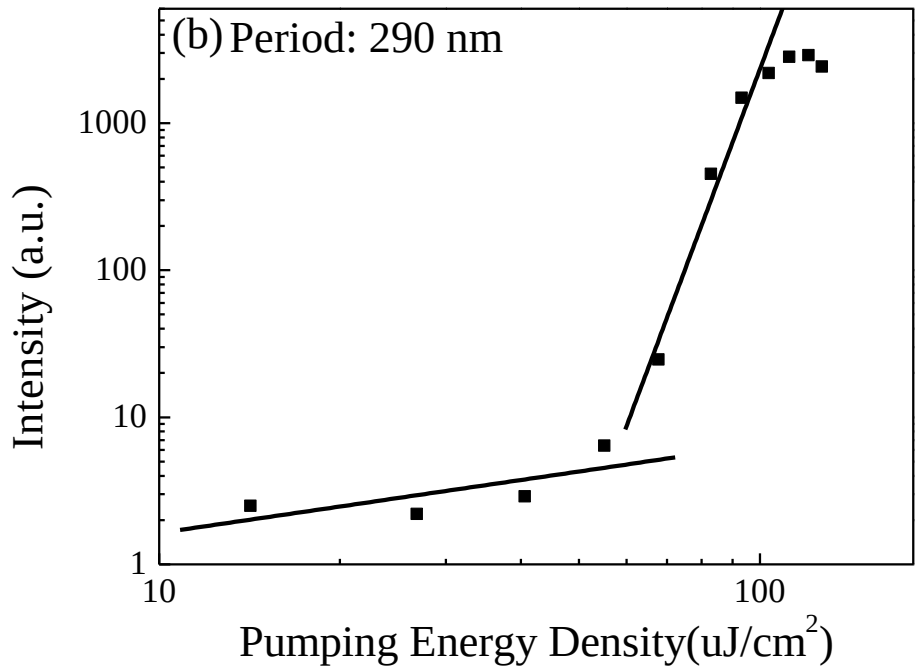
(b) Period: 290 nm
Intensity (a.u.)
1000
100
10
1
10
100
Pumping Energy Density(uJ/cm2)

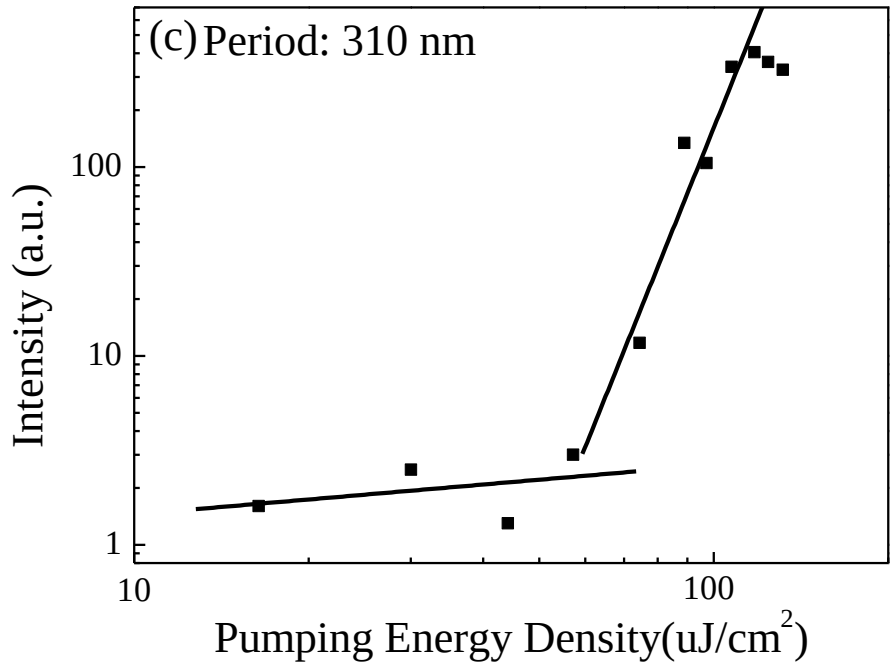

Fig.5.6 Output intensity as a function of pumping energy density of DFB laser with (a) 270 nm periods; (b)290 nm periods; (c)310 nm periods.

Fig. 5.6 shows the output intensity of the three DFB lasers as a function of pumping energy density. As observed, the intensity increases with increasing pumping energy density and a clear abrupt change occurred when the pumping energy density is above the threshold. The thresholds of the DFB lasers are in the range 70-80 $\mu J/cm^2$. With different periods of gratings, the laser emission peaks varied but the thresholds remained unchanged. Comparing to Section 4.3.2, the thresholds of DFB laser using PFO as the gain medium were about half that of ASE_{PFO} , showing that the threshold can be greatly reduced by DFB structure. The largest output intensity achieved was 3242 a.u. for the device using 270 nm period of grating while the performance of the one with 290 nm period was comparable (2894 a.u.). However, the sample with grating period 310 nm gave the lowest intensity (450 a.u.), about six times less than the others.

These results have confirmed the ability of manipulating light emission using DFB structure to tune the location of emission peak. However, the peak intensity is strongly dependent on the overlapping between PFO emission and lasing mode (the peak in Fig.5.2). From the PL emission spectrum of PFO (Fig.4.4), the dominant intensity ranges from 420 nm to 460 nm. Thus, even though the light amplification by DFB structure with grating period 310 nm could increase the intensity of light, the output light intensity at wavelength 480 nm would still be relatively low comparing to the others. Therefore, it is important to select appropriate grating period (i.e. lasing mode) to match the emission of gain medium, in order to achieve sufficient lasing intensity. In contrast, the other two DFB laser peaks are located exactly in the range of the dominant intensity of PFO emission, thus resulting in higher output intensity. These results also agreed with the simulation (Fig.5.3). In short, lasing emission was demonstrated using 2D DFB structure, which could provide strong light amplification. The laser emission peak can be tuned, and the threshold can be reduced using DFB structure.

CHAPTER 6 UNPOLARIZED LASING EMISSION FROM ORGANIC MICROCAVITY

In this chapter, lasing was demonstrated using microcavity structure. Laser emission was produced by an optically pumped active layer, PFO, sandwiched between a distributed Bragg reflector (DBR) and an aluminum (Al) mirror. The threshold of this microcavity organic laser was 145 μJ/cm^2 and the line-width was 5 nm. The polarization of the laser emission was also investigated that non-polarized lasing signal was observed.

6.1 Distributed Bragg mirror

A DBR-metal mirror was employed in the microcavity structure. DBR mirror is able to provide high reflectance in visible region to increase the Q-factor of laser cavity. The DBR substrate was composed of multi-layers of SiO_2 (60nm) and Ta_2O_5 (75nm) on amorphous glass. This DBR was designed by us and fabricated by a commercial company. There were 15 pairs of alternating SiO_2 and Ta_2O_5, where the number of pairs was determined by simulation. In Section 2.4.3, we showed that an increase in the numbers of alternating layers yielded improved reflectance with more well-defined band width. Therefore, it is necessary to have sufficient pair layers to achieve high-quality cavity.

Simulation was carried out to determine the optimum conditions of the DBR in for fabricating the laser cavity. The simulation was based on transfer matrix method (Section 2.4.3) modeling with varied numbers of pairs of alternating SiO_2 (60nm) and Ta_2O_5 (75nm) layers using MATLAB software. The refractive indices of Ta_2O_5 and SiO_2 were measured by the ellipsometry (section 3.5.2). The calculated transmission spectra of DBR with 5, 10 and 15 pairs are presented in Fig. 6.1. Considering the

spectral range from 440 nm to 530 nm, it is obvious that increasing the number of pairs would decrease the transmission of the stop-band (i.e. the region with relatively low transmittance) and resulted in sharper transmission cut-off. Moreover, compared to 5 and 10 pairs the transmittance of the DBR with 15 pairs approaches 0% and has longer stop band, which implies high reflection within this stop-band assuming no absorption in Ta_2O_5 and SiO_2 layers. Beyond the region of the stop-band the rippling transmission curves are due to constructive interference of multiple reflections in each layer. These results demonstrated that using 15 pairs of alternating Ta_2O_5 and SiO_2 layers for the DBR substrate would give high reflection (nearly 100%). So it would be suitable to be used as a high quality reflected mirror. Since PFO was used as the gain medium of the microcavity organic layer in this work, it would be important that the emission peak of PFO (~450nm) lies within the stop-band of the DBR.

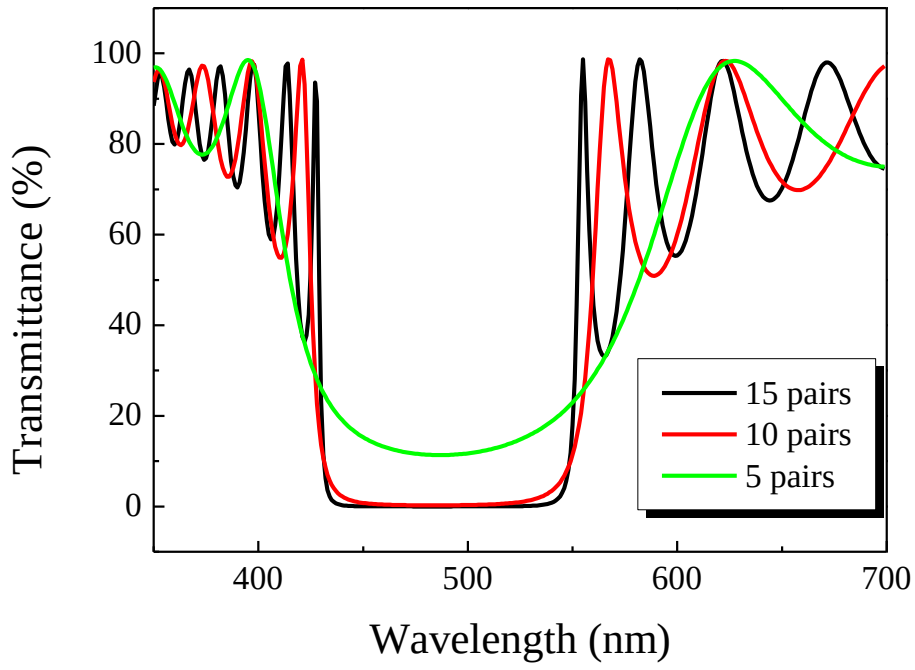

Fig. 6.1 Calculated transmittance of DBR with varied numbers of pairs (5, 10, and 15) of alternating Ta_2O_5 and SiO_2 layers.

The transmission spectrum of the prepared DBR substrate with 15 pairs of alternating Ta_2O_5 and SiO_2 layers was measured to compare with simulation (Fig. 6.2). The measured spectrum agrees very well with the calculation, especially in the stop-band. Beyond the stop-band, the interference patterns of the measured and calculated spectra are almost identical. The wavelength of the pumping laser in this work was 355 nm. From the measurement, the transmittance of the DBR at 355 nm is 84%. It is considered acceptable for the incident laser beam to reach the gain medium without significant loss.

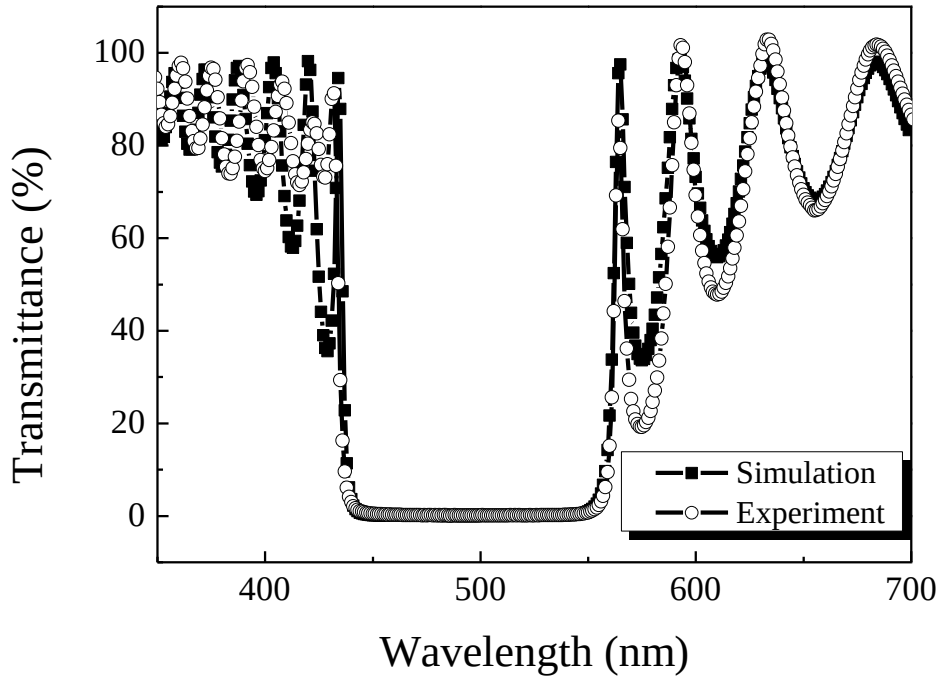

Fig. 6.2 Measured and calculated transmission spectra of DBR with alternating Ta_2O_5 and SiO_2 layers.

6.2 Cavity design

Microcavity techniques are widely used in solid state laser devices [21-23, 73-77]. The aim of this study was to enhance light-matter interaction via microcavity laser to achieve high power density. This would facilitate-electrical pumping. The

most common approach is to enhance the Q-factor of the device [23, 88]. That is, increasing the reflectivity of the dielectric or metal mirror in the laser cavity to enlarge the path length of effective photon and lower the threshold energy.

Apart from optimizing the number of alternating layers in the DBR, it was necessary to determine the optimum thickness of the active medium (i.e. PFO) because it would affect the cavity mode for lasing in the microcavity laser. The structure in simulation was glass / DBR / PFO / Al. The thickness of PFO was the varying parameter while the DBR was fixed with 15 pairs of alternating Ta_2O_5 and SiO_2 layers and the thickness of Al was 30 nm. There is purpose of using 30 nm Al. It is to ensure the device having sufficient reflection to act as reflected mirror, while the laser emission can be barely emitted from the device. The refractive indices of Ta_2O_5, SiO_2 and Al were measured by the ellipsometry. For simplification, it was assumed that the extinction coefficient of Ta2O5 and SiO2 equal to zero. But it may lead to varied overall transmittance in simulation and experiment. The level of transmittance may have ~30% difference between simulation and experiment. And the purpose of using simulation is to confirm the position of cavity mode, so the difference of transmittance will not affect the comparison.

The calculated transmission spectra of the designed structure are depicted in Fig. 6.3(a). The thickness of PFO is 70 nm, 90 nm and 110 nm. Similar to Fig. 6.2 constructive interference appears beyond the stop-band. Besides that, the overall transmittance of the constructive interference region decreases with increasing PFO thickness. It is due to increasing absorption of PFO. The variation in PFO thickness also affects the stop-band. Because of cavity effect, cavity mode was induced in the designed structure, which is represented by the peaks within the region of the stop-band of the spectra. Laser emission is strongly depended on cavity mode. It is important that the cavity mode sufficiently overlaps with the emission of the gain

medium for lasing. The emission peak of PFO is 450 nm (Section 4.1.2). Therefore, it is desirable to tune the cavity mode at or near 450 nm. In Fig. 6.3 (a), the cavity mode alters by the thickness of PFO. The peaks of the cavity mode are 430 nm, 450 nm and 478 nm corresponding to PFO thickness 70 nm, 90 nm, and 110 nm respectively. Therefore 90 nm of PFO would have the best overlapping between the cavity mode and PFO emission.

However, 90 nm is not the only thickness of PFO for a cavity mode occurring at 450 nm. When the thickness of PFO is increased to 235 nm, the cavity mode appears at 450 nm as well (Fig. 6.3(b)). In fact, the cavity mode at 450 nm would occur repeatedly with specific thicknesses. Compared to Fig. 6.3(a), similar results are obtained as shown in Fig. 6.3(b) where the peaks of the cavity mode are 431 nm, 450 nm and 471 nm corresponding to PFO thickness 210 nm, 235 nm, and 260 nm respectively. The repeated cavity mode with different thickness can be explained by the equation 2.8 in Section 2.4.3. The equation 2.8 shows that by increasing the cavity length, that is the gain medium thickness, the cavity mode wavelength can be the same while the orders of the mode are different.

The thickness of 235 nm was selected for the PFO layer in this work for two reasons; comparing the two cavity modes corresponding to PFO thickness 90 nm and 235 nm, the latter would give a cavity mode with narrower full-width half-maximum (FWHM), which suggests a higher Q-factor of the device. Thus the quality and efficiency of the device would be improved when using 235 nm of PFO. Besides that, there are other thicknesses of PFO (>235 nm) inducing cavity mode at 450 nm. But a thick gain medium would lead to multiple modes for laser emission (Fig.6.3(c)). In Fig.6.3(c), there are multiple modes inside the stop band. It will lead to decreased efficiency of laser emission, because the output intensity will distributed in several modes. Therefore, the thickness of the PFO layer should be constrained to 235 nm.

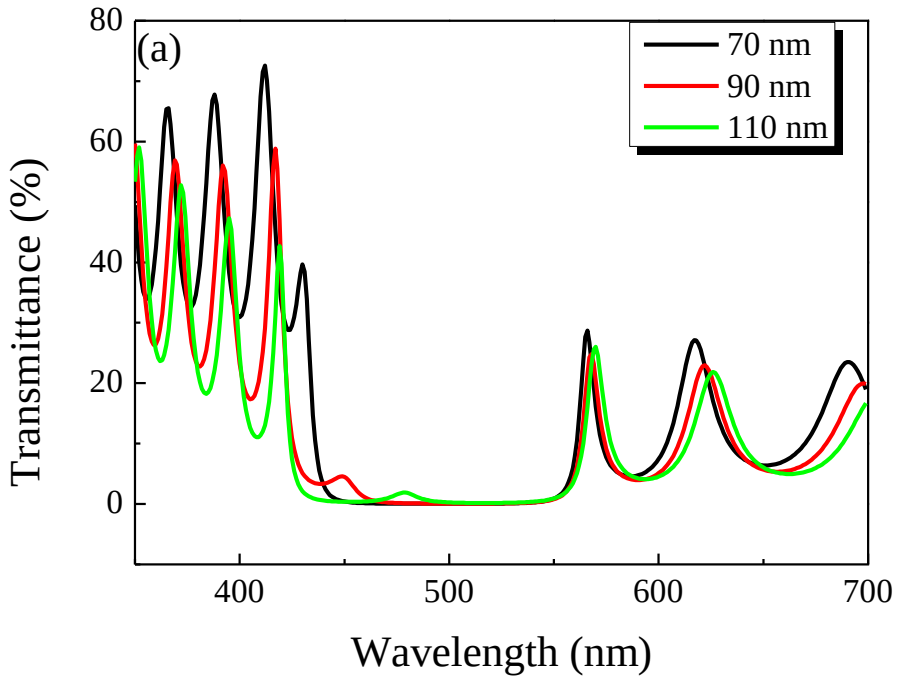
(a)
70 nm
90 nm
110 nm
Transmittance (%)
Wavelength (nm)
0
20
40
60
80
400
500
600
700

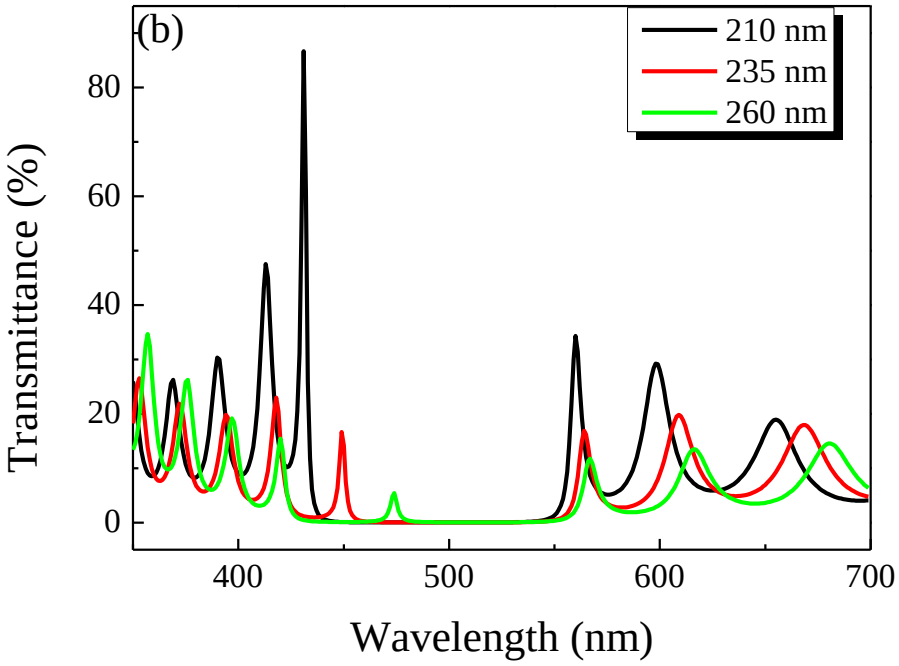
(b)
210 nm
235 nm
260 nm
Transmittance (%)
Wavelength (nm)
0
20
40
60
80
400
500
600
700

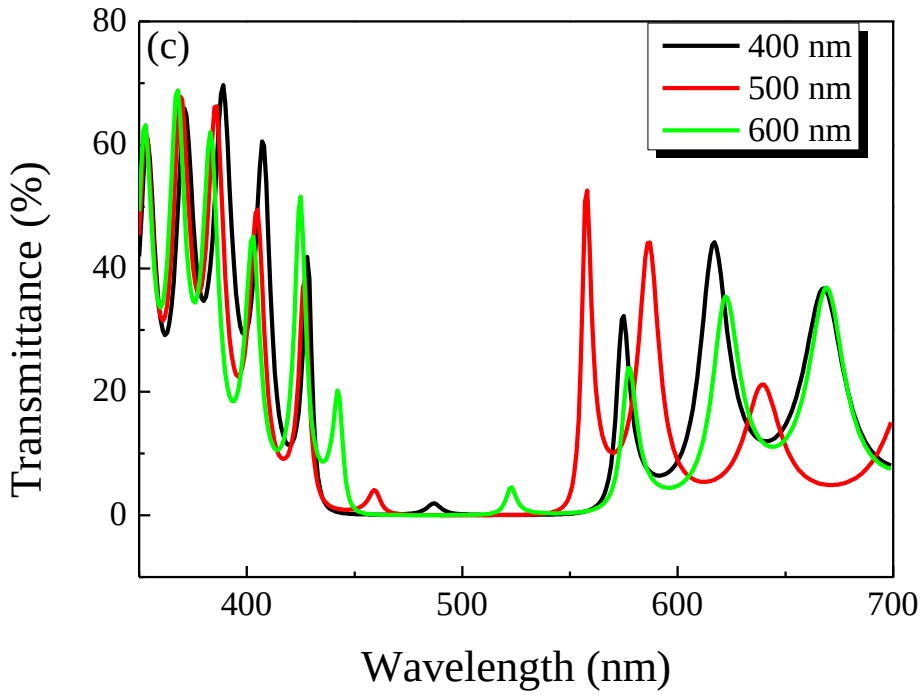

Fig. 6.3 Calculated transmission spectra of microcavity with PFO thickness (a) 70 nm, 90 nm, and 110 nm; (b) 210 nm, 235 nm, and 260 nm; and 400 nm, 500 nm, and 600 nm.

A microcavity device was fabricated for laser measurement. A layer of PFO (220 nm) was deposited by spin-coating onto the surface of tailor-made DBR substrate, followed by a 30 nm Al mirror deposited by thermal evaporation. The thinner PFO in experiment was due to the spin-coating variation, while the experiment results did not show sufficient difference comparing to the simulation. The structure of the microcavity is depicted in Fig. 6.4.

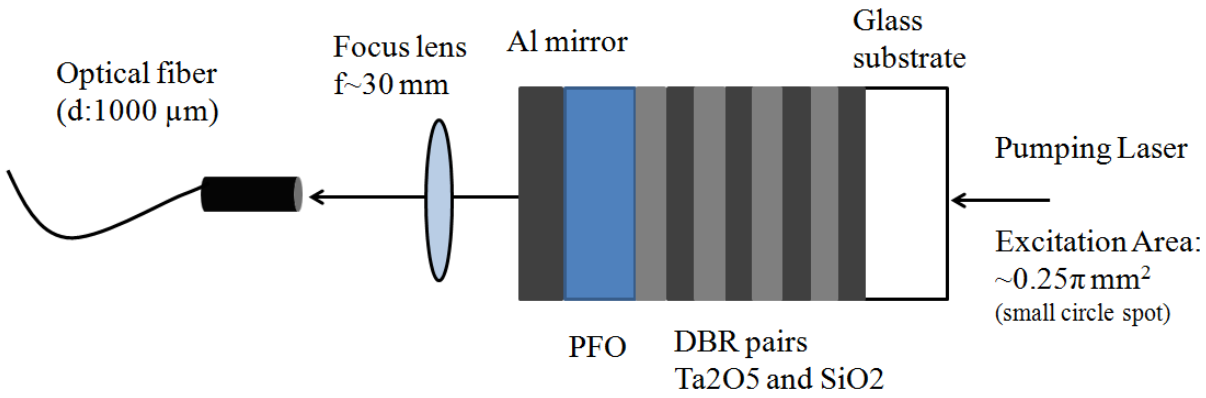

Fig. 6.4 Illustration of experimental setup and the structure of the microcavity laser.

Sturcture: glass / DBR (15 pairs of Ta_2O_5/SiO_2) / PFO (220 nm) /Al (30 nm).

The pumping laser mentioned in Section 3.4.4 was used in this experiment. In order to obtain strong signal, the setup was modified (Fig. 6.4). The position of the optical fiber to collect the laser signal was placed behind the Al mirror. That is, the pumping laser was first incident on the glass substrate and then passed through the DBR pairs into the PFO layer. Finally, the laser signal was received behind the Al mirror.

The transmittance of the cavity device was also investigated. The structure of the device was glass / DBR (15 pairs of Ta_2O_5/SiO_2) / PFO (220nm) /Al (30 nm). Fig. 6.5 compares the measured and simulated transmission spectra. The measured cavity mode in fact occurs at 440 nm within the stop-band, which would overlap well enough with PFO emission. The transmittance of the measured cavity mode is only 5%, which is favorable for laser emission. Since a low transmittance at 440 nm implies high reflection at that wavelength, the cavity would reflect the laser emission and so amplifying the light. The simulated cavity mode is consistent with the

experiment (Fig. 6.5). The higher transmittance in simulation may be due to assumption of zero materials absorption. In fact there are other losses arisen from metal and metal-organic interface, but these losses were not included in the simulation.

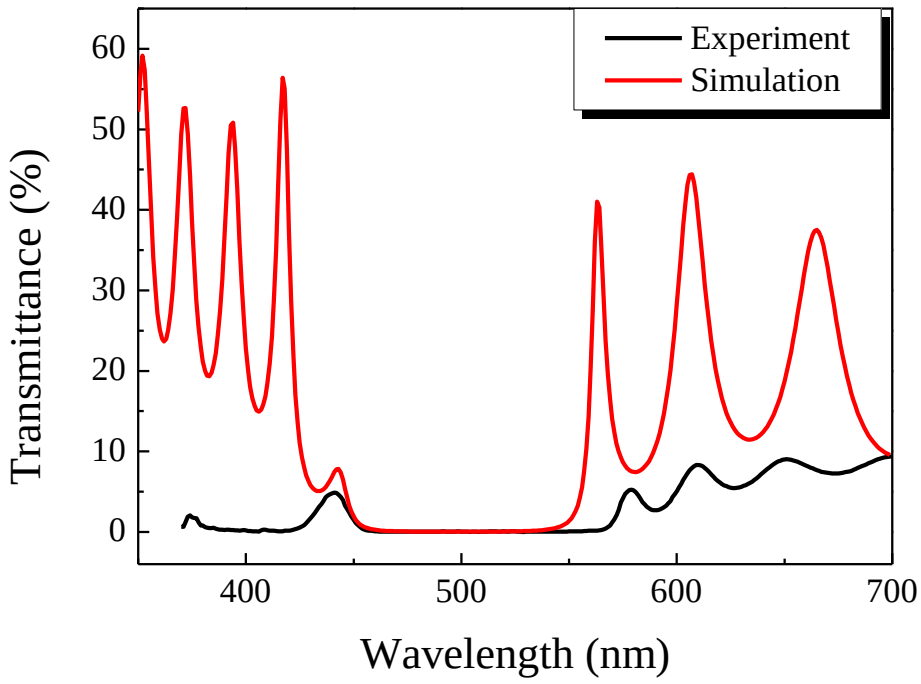

Fig. 6.5 Measured and simulated transmittance of cavity device. Sturcture: glass / DBR (15 pairs of Ta_2O_5/SiO_2) / PFO (220 nm) /Al (30 nm).

6.3 Lasing emission from microcavity laser

To evaluate the quality of laser emission of the microcavity laser, laser measurement with power dependence was used. These measurements were able to show the consistency of the device by optical pumping and the relationship between the transmission spectrum of the device and laser spectrum. The results showed the lasing characteristics of the laser emission, i.e. spectral narrowing and existence of threshold. Also, the polarization of lasing emission was investigated.

6.3.1 Lasing emission

The characteristics of lasing emission were investigated. The sample image captured by a microscope (20X) is shown in Fig. 6.6. The image is in orange-red color due to the reflection of the device because most of the color in blue and green regions is reflected (Fig. 6.5) Also the image shows uniform color distribution suggesting smooth sample surface.

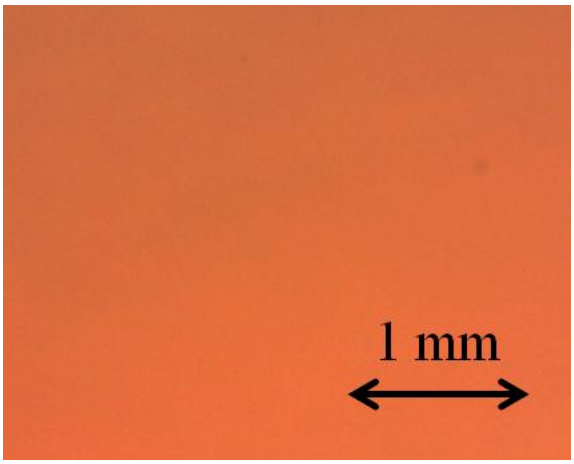

Fig. 6.6 Optical image of the cavity device. Sturcture: glass / DBR (15 pairs of Ta_2O_5/SiO_2) / PFO (220 nm) /Al (30 nm).

As mentioned before, the Al reflected mirror was designed to 30 nm in purpose to balance both transmission and reflection of the device. Actually, for proving the 30 nm of Al is the optimized thickness, 20 nm and 40 nm of Al devices were also fabricated. For DBR/ PFO (220 nm)/ Al (40 nm) device, using the same experimental setup, the laser signal was hard to be detected but only noise signal. It may because of too thick Al mirror, and the laser emission was difficult to transmit through the metal thin film. For the device with 20 nm Al, the signal can be received. However, the device performance was relatively low comparing to 30 nm Al. The FWHM of emission spectrum was around 10 nm (in Fig. 6.7) and the output intensity did not show a clear dramatically change. Device with 30 nm of Al showed better

performance with narrower FWHM and clear threshold. The performance of device with 20 nm of Al may affected by the thinner metal, and leading to lower reflection. Thus, the Q- factor of device was decreased and the efficiency was dropped. As a result, 30 nm of Al was chosen to be the thickness of reflected mirror.

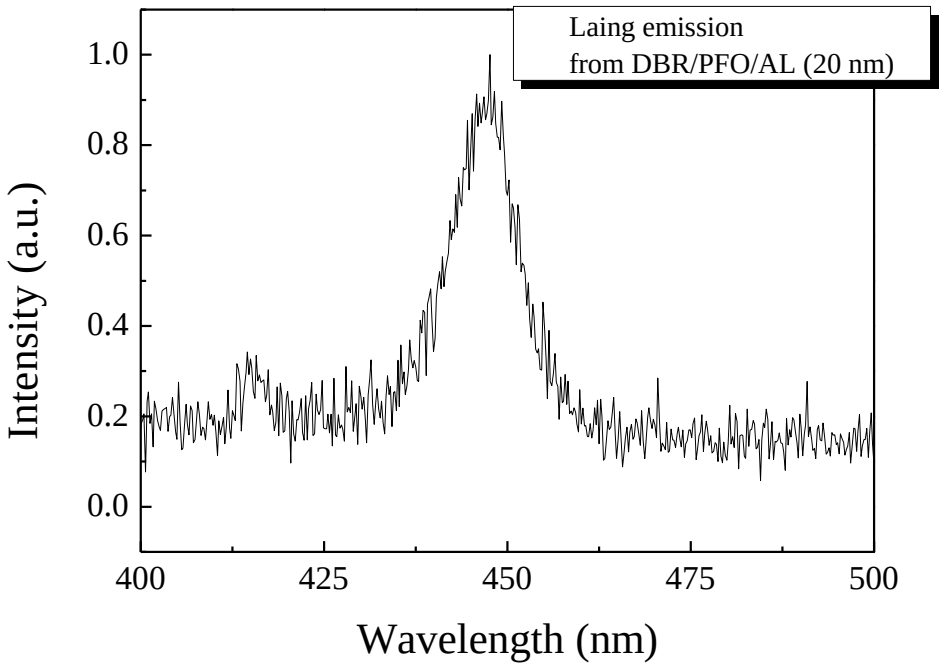

Fig. 6.7 Lasing emission spectrum (E= 204 μJ/cm^2) from the microcavity DBR/PFO (220 nm)/Al (20 nm).

Apart from the thickness of metal, the kind of metal was studied. Ag was also chosen to be the reflected mirror, as its high reflection in visible range. The fabricated device was DBR/PFO (220 nm)/ Ag (30 nm). The result showed the threshold was 140 μJ/cm^2, which is comparable to device with 30 nm Al. But for the convenience of fabrication, the Al thin film was still chosen.

In device DBR (15 pairs of Ta_2O_5/SiO_2) / PFO (220 nm) /Al (30 nm), the transmission spectrum of the microcavity (Fig. 6.5) is used to compare with the measured laser spectrum above the threshold energy (pumping energy E = 204 μJ/cm^2)

(Fig. 6.8). The laser emission was dominated by the high gain with the peak at 444 nm, which was correlated to the cavity mode at 441 nm; and spectral narrowing is observed with FWHM reducing from 16 nm to 5 nm.

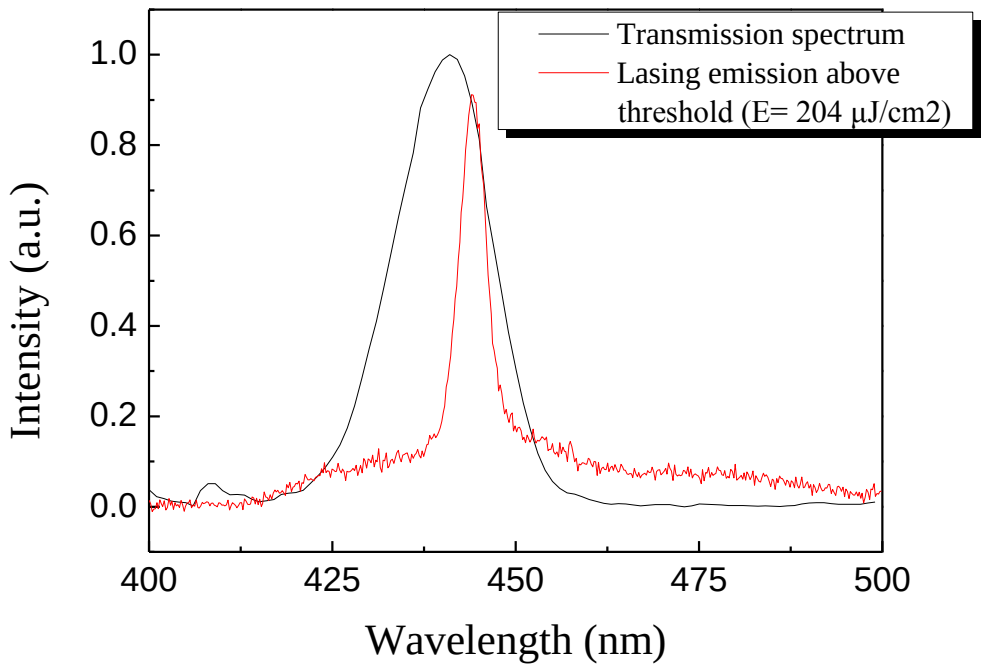

Fig. 6.8 Transmission and lasing emission spectrum (E= 204 µJ/cm^2) from the microcavity DBR/PFO (220 nm)/Al (30 nm).

The laser emission spectra of the cavity device with varied pumping energies (from 64 µJ/cm^2 to 240 µJ/cm^2) are shown in Fig. 6.9. All emission peaks locate at 444 nm. At low pumping energy (below 145 µJ/cm^2), no lasing spectra were measured. The rapid change in the spectra with the cavity mode (λ = 441 nm) at the emission peak (λ = 444 nm) is dominating the laser emission at higher pumping energy (above 145 µJ/cm^2). The spectral width corresponds to a Q-factor of 89. It is not considered a high Q-factor comparing to conventional laser [20, 48, 51]. It may be due to using thin layer of Al (30 nm) as one of the reflected mirrors since the Al mirror has relatively low reflectivity in comparison to the DBR pairs. Nevertheless,

the Q-factor was improved comparing to the approach to induce laser emission in Section 4.2 in which fused silica substrate and air were used as the cavity resulting in relatively low Q-factor. Here, in the microcavity structure DBR-metal mirror was employed, where the DBR could give high reflectance in visible region leading to increased Q-factor. Besides, the stimulated emission was dominating and hence the emission of the cavity device was considered lasing. Because the spectra are not simply proportional to pumping energy and the laser emission is mode-dependent. If there was no gain or simulated emission, there would have been no dramatic change and mode-guided emission.

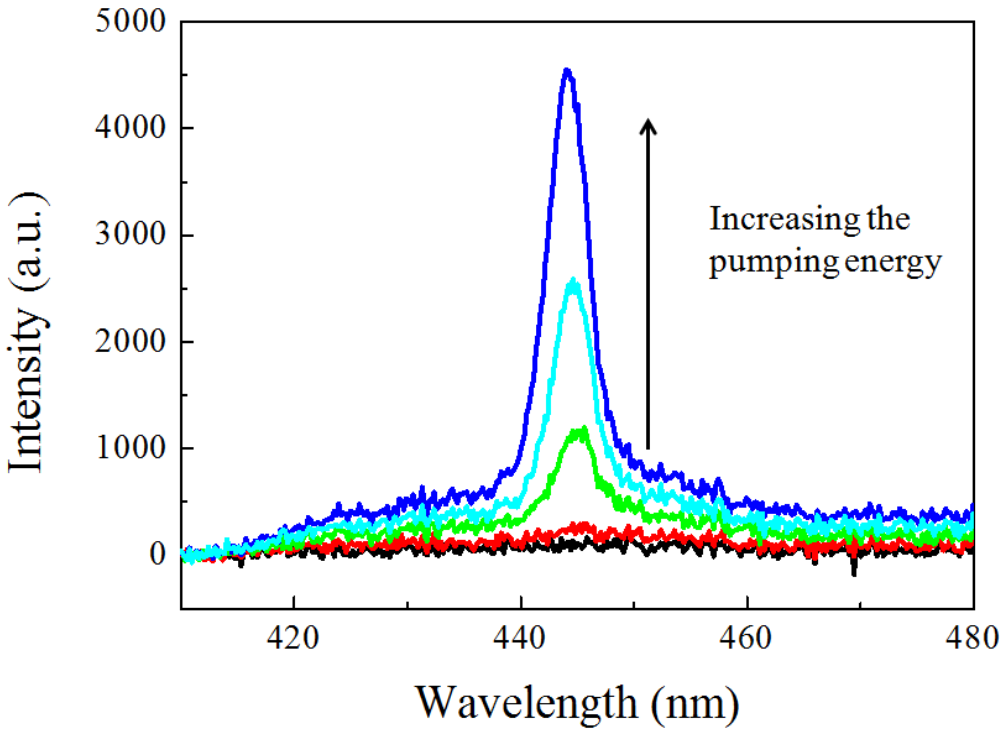

Fig. 6.9 Lasing emission spectra from the microcavity at different pumping energy.

The polarization of the laser emission was also studied, as there is not much discussion on polarization state of cavity laser. The polarization of light was measured in transverse electric (TE) and transverse magnetic (TM). While the laser emission was measured in both TE and TM polarizations, the pumping laser was in TM

polarization. The laser emission of the device was non-polarized as suggested by Fig. 6.10, i.e. nearly identical laser emission spectra in TE and TM polarizations. In our device, since there was no polarized element or structure inside the cavity, the gain medium was uniformly excited and emitted light with random polarization and direction.

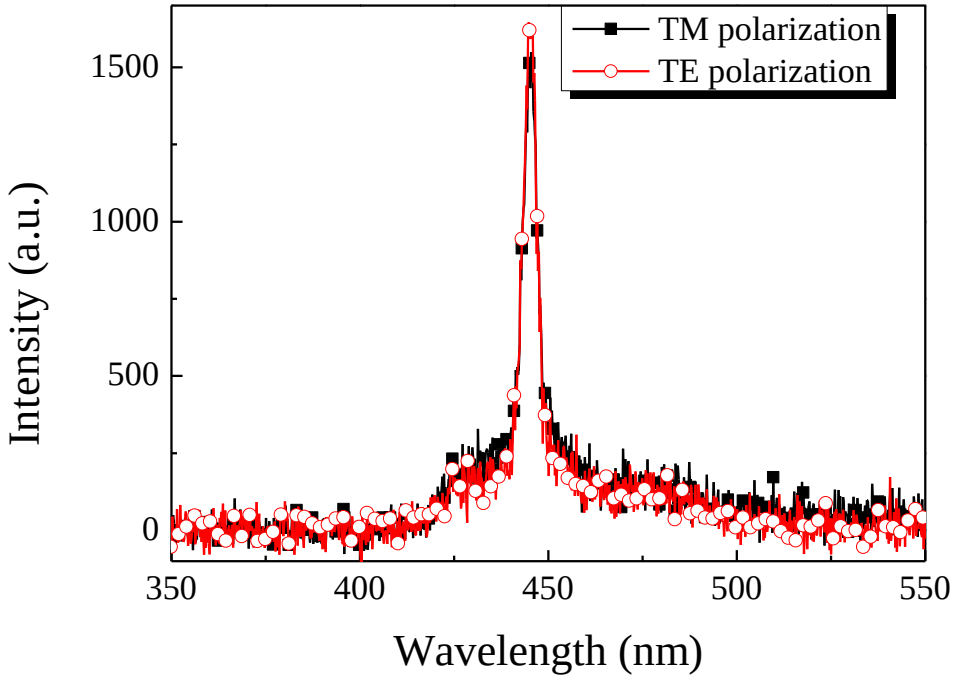

Fig. 6.10 Laser emission spectrum in cavity device in TE and TM polarization.

6.3.2 Energy dependence

The efficiency measurement described in Section 3.5.1 was used to measure the power dependence of the cavity device. The power dependence of the laser output and input for excitation was used to determine the threshold energy of the microcavity laser and how efficient it is. Fig. 6.11 is the output intensity of the cavity laser as a function of pumping energy density. The threshold of the pumping energy density is 145 μJ/cm^2, which is confirmed the existence of the laser emission. Comparing to the edge-emitting organic lasing device in Section 4.3.2, the threshold is comparable to

each other. It is expected that the cavity device would have lower threshold than the edge-emitting organic lasing device, because the Q factor of the cavity laser is larger than that of edge-emitting organic lasing device (the Q factor of edge-emitting organic laser device is near zero, as one of the reflected mirror is air.). However, it was not the case. It is due to higher optical loss in the cavity device and a short gain length in the cavity structure in this part of the work. Moreover, using metal as the reflected mirror would lead to higher optical loss. So, the higher pumping energy density was required to overcome the optical loss. Although the higher pumping energy density was required in the device, by adding the metal still can open the possibility of organic laser in electrical pumping. The thin metal may used to be the electrode of the laser to inject the electron.

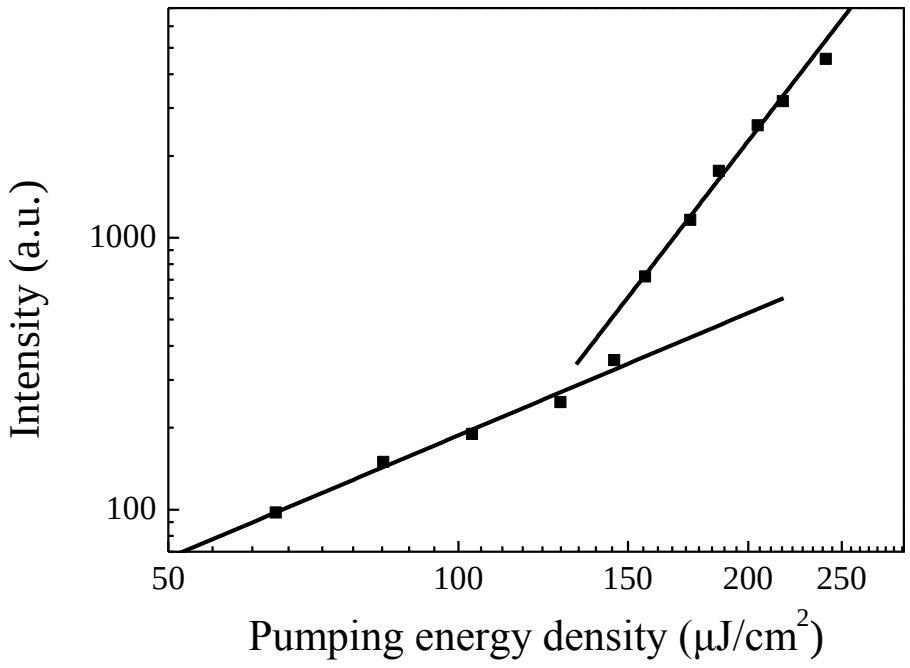

Fig.6.11 Output intensity as a function of pumping energy density of the microcavity laser.

CHAPTER 7 CONCLUSION

In this thesis, we investigated the amplified spontaneous/ stimulated emission characteristics of organic laser under optical pumping using designed structure. DFB and cavity structures were used to enhance Q factor and lower the threshold. Various measurement techniques were developed in order to explore the lasing properties of the organic laser.

In this study, PFO and F8BT were used as the gain medium in organic lasers since they can achieve ASE under optical pumping relatively easy. DFB and cavity structure were employed to improve the lasing properties. Both methods can increase the Q factor of the laser up to ~300. Besides, it was demonstrated that using DFB and cavity structure can give precise control on the laser emission wavelength. Also, FDTD simulation was used to predict the wavelength of laser emission and consistent with the experimental results.

Using DFB and cavity structures in the organic lasers, the threshold was reduced. The laser with cavity showed comparable energy level of threshold comparing with neat film of PFO. It was because of the high optical loss in metal-organic interface. In contrast, DFB organic laser showed significant reduction of threshold by two times from 130 $\mu J/cm^2$ to 70 $\mu J/cm^2$comparing with the neat film of PFO. Without the interface loss, the grating has highly enhanced the light amplification leading to lower threshold.

Moreover, the polarization characteristic of laser emission from cavity laser was investigated, which is not emphasized in other similar research. With DBR-metal mircocavity, the laser emission is non-polarized. It is because there is no polarized element or structure was inserted, and thus having a randomly polarized laser

emission. For DFB laser, the polarization of output laser beam has been studied by the other groups [89]. With the periodic and directional structures, the laser beam showed the polarization which was parallel to the designed directional structure. So we did not focus in polarization of DFB laser, but cavity laser.

A novel sample design was developed to study the tunability of laser emission. The design consisted of two cascaded organic films, PFO and F8BT. Both polymers were shown that in optical pumping they showed efficient performance. The device has spontaneous twin ASE and the overlapping of two emission allows the tuning ASE color from blue, white and green continuously through the spatially selection of the directional ASE. The continuously tunability of ASE has a linear relationship in CIE coordinates. Furthermore, the device is sensitive to vibration along the optical path between device and the detector showing the potential to be a vibration detector.

In conclusion, organic lasers and organic amplified emission have been demonstrated using different structures, including neat thin film of polymer, DFB structure and DBR-metal cavity structure. The characterizations of each laser were investigated, showing that the threshold can be decreased by using different laser resonator and lead to the possibility of electrical pumping. Also a novel structure for tunable color of laser emission was proposed. For future work, it is possible to use the cavity design with DFB structure to the basis of organic laser using electric current injection. While the Q factor can be further improved by DBR cavity, using the DFB structure in the cavity with ultra-thin metal could significantly reduce scattering loss.

LIST OF REFERENCES

1. D. Moses, “High quantum efficiency luminescence from a conducting polymer in solution: A novel polymer laser dye,” Appl. Phys. Lett. **60**, 3215, (1992).
2. F. Hide, M. A. DiazGarcia, B. J. Schwartz, M. R. Andersson, Q. B. Pei, and A. J. Heeger, “Semiconduting Polymers: A New Class of Solid-State Laser Materials,” Science, **273**, 1833, (1996).
3. N. Tessler, “Lasers based on semiconducting organic materials,” Adv. Mater. **11**, 363, (1999).
4. M. D. McGehee and A. J. Heeger, “Semiconducting (conjugated) Polymers as Materials for Solid State Lasers,” Adv. Mater. **12**, 1655, (2000).
5. I. D. W. Samuel, and G. A. Turnbull, “Organic Semiconductor Lasers,” Chem. Rev. **107**, 1272, (2007).
6. N. Tessler, G. J. Denton, and R. H. Friend, “Lasing from conjugated-polymer microcavities,” Nature **382**, 695 (1997).
7. G.J. Denton, N. Tessler, N.T. Harrison, R.H. Friend, “Factors Influencing Stimulated Emission from Poly (p-phenylenevinylene),” Phys. Rev. Lett. **78**, 733, (1997).
8. M. Koschorreck, R. Gehlhaar, V. G. Lyssenko, M. Swoboda, M. Hoffmann, and K. Leo, “Dynamics of a high Q vertical cavity organic laser,” Appl. Phys. Lett. **87**, 181108, (2005).
9. George Heliotis, Ruidong Xia, Graham A. Turnbull, Piers Andrew, William L. Barnes, I. D. W. Samuel, and Donal D. C. Bradley, “Emission Characteristics and Performance Comparison of Polyfluorene Lasers with One and Two Dimensional Distributed Feedback,” Adv. Funct. Mater. **14**, 91, (2004).
10. R. Xia, G. Heliotis, P. N. Stavrinou and D. D. C. Bradley, “Polyfluorene distributed feedback lasers operating in the green-yellow spectral region,” Appl. Phys. Lett. **87**, (2005).
11. S. V. Frolov, M. Shkunov, and Z. V. Vardeny, “Ring microlasers from conducting polymers," Phys. Rev. B, **56**, 4363, (1997).
12. Guichuan Xing, Nripan Mathews, Swee Sien Lim, Natalia Yantara, Xinfeng Liu, Dharani Sabba, Michael Gratzel, Subodh Mhaisalkar, and Tze Chien Sum, “Low temperature solution processed wavelength tunable perovskites for lasing,” Nature materials, **13**, 476, (2014).
13. H. Kogelnik and C.V. Shank, Applied Physics Letters, **18**, 152 (1971).
14. C. Bauer, H. Giessen, B. Schnabel, E.B. Kley, C. Schmitt, U. Scherf and R.F.Mahrt, Advanced Materials, **13**, 1161 (2001).

15. Ankun Yang, Thang B. Hoang, Montacer Dridi, Claire Deeb, Maiken H. Mikkelsen, George C. Schatz, and Teri W. Odom, “Real time tunable lasing from plasmonic nanocavity arrays,” Nature communications, **7939**, (2015).
16. I. D. W. Samuel, and G. A. Turnbull, “Organic Semiconductor Lasers,” Chem. Rev. **107**, 1272, (2007).
17. M. Yan, L. J. Rothberg, F. Papadimitrakopoulos, M. E. Galvin, and T. M. Miller, “Spatially indirect excitons as primary photoexcitations in conjugated polymers,” Phys. Rev. Lett. **72**, 1104, (1994)..
18. B. J. Schwartz, F. Hide, M. R. Andersson, and A. J. Heeger, “Ultrafast studies of stimulated emission and gain in solid films of conjugated polymers,” Chem. Phys. Lett. **265**, 327, (1997).
19. G. J. Denton, N. Tessler, N. T. Harrison, and R. H. Friend, “Factors influencing stimulated emission from Poly(p-phenylenevinylene),” Phys. Rev. Lett. **78**, 733, (1997).
20. V. G. Kozlov, G. Parthasarathy, P. E. Burrows, V. B. Khal_n, J. Wang, S. Y. Chou, and S. R. Forrest, “Structures for organic diode lasers and optical properties of organic semiconductors under intense optical and electrical excitations," IEEE Journal of Quantum Electronics, **36**, 18, (2000).
21. I.D.W. Samuel, “Fantastic plastic," Nature, **429**, 709, (2004).
22. H. Shirakawa, E. J. Louis, A. G. Macdiarmid, C. K. Chiang, and A. J. Heeger, “Synthesis of Electrically Conducting Organic Polymers: Halogen Derivatives of Polyacetylene, (CH)x,” J. C. S. Chem. Comm. **16**, 578, (1977)..
23. C. K. Chiang, C. R. Fincher, Y. W. Park, A. J. Heeger, H. Shirakawa, E. J. Louis, S. C. Gau, and A. G. Macdiarmid, “Electrical Conductivity in doped Polyacetylene,” Phys. Rev. Lett. **39**, 1098, (1977).
24. http://nobelprize.org/nobel_prizes/chemistry/laureates/2000/public.html
25. C.W. Tang, and S.A. Vanslyke, “Organic electroluminescent diodes,” Appl. Phys. Lett. **51**, 913, (1987).
26. J.H. Burroughes, D.D.C. Bradley, A.R. Brown, R.N. Marks, K. Mackay, R.H. Friend, P.L. Burns, and A.B. Holmes, “Light-emitting diodes based on conjugated polymers," Nature, **347**, 539, (1990).
27. A.J. Heeger, “Light emission from semiconducting polymers: light emitting diodes, light-emitting electrochemical cells, lasers and white light for the future," Solid State Commun. **107**, 673, (1998).
28. Y. Xiong, L. Wang, W. Xu, J. Zou, H. Wu, Y. Xu, J. Peng, J. Wang, Y. Cao, and G. Yu, “Performance analysis of PLED based at panel display with RGBW sub-pixel layout," Organic Electronics, **10**, 857, (2009).
29. K. Saxena, V. K. Jain, and D. S. Mehta, “A review on the light extraction

techniques in organic electroluminescent devices," Optical Materials, **32**, 221, (2009).

30. S. Gunes, H. Neugebauer, and N.S. Sariciftci, "Conjugated polymer-based organic solar cells," Chem. Rev, **107**, 1324, (2007).
31. T. Ameri, G. Dennler, C. Lungenschmied, and C. J. Brabec, "Organic tandem solar cells: A review," Energy & Environmental Science, **2**, 347, (2009).
32. Y. Yao, Y. Liang, V. Shrotriya, S. Xiao, L. Yu, and Y. Yang, "Plastic near-infrared photodetectors utilizing low band gap polymer," Adv. Mater, **19**, 3979, (2007).
33. X. Gong, M. Tong, Y. Xia, W. Cai, J.S. Moon, Y. Cao, G. Yu, C. L. Shieh, B. Nilsson, and A. J. Heeger, "High-Detectivity Polymer Photodetectors with Spectral Response from 300 nm to 1450 nm," Science, **325**, 1665, (2009).
34. A. Tsumura, H. Koezuka, and T. Ando, "Macromolecular electronic device: Field-effect transistor with a polythiophene thin film," Appl. Phys. Lett. **49**, 1210 (1986).
35. B. Crone, A. Dodabalapur, Y. Y. Lin, R. W. Filas, Z. Bao, A. LaDuca, R. Sarpeshkar, H. E. Katz, and W. Li, "Large-scale complementary integrated circuits based on organic transistors," Nature, **403**, 521, (2000).
36. E. C. P. Smits, S. G. J. Mathijssen, P. A. van Hal, S. Setayesh, T. C. T. Geuns, K. A. H. A. Mutsaers, E. Cantatore, H. J. Wondergem, O. Werzer, R. Resel, M. Kemerink, S. Kirchmeyer, A. M. Muzafarov, S. A. Ponomarenko, B. de Boer, P. W. M. Blom, and D. M. de Leeuw, "Bottom-up organic integrated circuits," Nature, **455**, 956, (2008).
37. Ruidong Xia, George Heliotis, and D. C. Bradley, "Fluorene-based polymer gain media for solid-state laser emission across the full visible spectrum," Appl. Phys. Lett. **82**, 3599 (2003).
38. Georgios Tsiminis, Yue Wang, Paul E. Shaw, Alexander L. Kanibolotsky,Igor F. Perepichka, Martin D. Dawson, Peter J. Skabara, Graham A. Turnbull1, and Ifor D. W. Samuel, "Low-threshold organic laser based on an oligofluorene truxene with low optical losses," Appl. Phys. Lett. **94**, 243304 (2009).
39. Y. kawamura, H. Yamamoto, K. Goushi, H. Sasabe, C. Adachi, H. Yoshizaki, "Ultraviolet amplified spontaneous emission from thin films of 4,4'-bis(9-carbazolyl)-2,2'-biphenyl and the derivatives," Appl. Phys. Lett. **84**, 2724 (2004).
40. G. Heliotis, D. C. Bradley, G. A. Turnbull, and I. D. W. Samuel, "Light amplification and gain in polyfluorene waveguides," Appl. Phys. Lett. **81**, 415 (2002).
41. I. D.W. Samuel, Ebinazar B. Namdas and Graham A. Turnbull, "How to

recognized lasing," Nature Photonics **3**, 546, (2009).

42. V. G. Kozlov, P. E. Burrows, G. Parthasarathy, and S. R. Forrest, "Optical properties of molecular organic semiconductor thin films under intense electrical excitation," Appl. Phys. Lett. **74**, 1057, (1999).
43. H. Shirakawa, E.J. Louis, A.G. Macdiarmid, C.K. Chang and A.J. Heeger, "Synthesis of electrically conducting organic polmer: halogen derivatives of polyacetylene, (CH)x," J. Chem. Soc., Chem. Commun. **16**, 578, (1977).
44. F. J. Duarte, and L. W. Hillman, "Dye laser Principles with applications," Academic Press, (1990)
45. W. Schnabel, "Polymers and light Fundamentals and Technical applications," Wiley-VCH, (2007).
46. I. D. W. Samuel, and G. A. Turnbull, "Polymer laser: recent advances," Materials today, **7**, 28, (2004).
47. W. Y. Liang, "Excitons," Physics Education, **5**, 226, (1970).
48. J. Franck, "Elementary processed of photochemical reactions," Transactions of the Faraday Society, **21**, 536, (1926).
49. Albert Sprague Coolidge, Hubert M. James, and Richard D. Present, "A study of the Franck-Condon Principle," Journal of Chemical Physics, **4**, 193, (1936).
50. Yehuda B. Band, "Light and Matter Electromagnetism, Optics, Spectroscopy and Lasers," John Wiley & Sons Ltd, (2007).
51. Kendric Smith, 2014, Basic Photochemistry, Photobiological Sciences Online (KC Smith, ed.) American Society for Photobiology, http://www.photobiology.info/ (reproduced with permission from Kendric Smith)
52. B. Schweiter, G. Wegmann, H. Giessen, D. Hertel, H. Bassler, and R. F. Mahrt, "The optical gain mechanism in solid conjugated polymers," Appl. Phys. Lett. **72**, 2933, (1998).
53. O. Svelto, "Principle of Laser," Springer, (2010)
54. A. Einstein, "The quantum theory of radiation," Physikalische Zeitschrift, **18**, 121 (1917).
55. Richard S. Quimby, "Photonics and laser an introduction," John Wiley & Sons, (2006).
56. Joseph T. Verdeyen, "Laser electronics," Prentice Hall, (2000).
57. Siegman, "Laser," Mill Valley, (1986).
58. Y. Sorek, R. Reisfeld, I. Finkelstein, and S. Ruschin, "Light amplification in a dye-doped glass planar waveguide," Appl. Phys. Lett. **66**, 1168, (1995).
59. Michael D. McGehee, Rahul Gupta, Siegfried Veenstra, E. Kirk Miller, Maria A. Diaz-Garcia, and Alan J. Heeger, "Amplified spontaneous emission from photopumped films of a conjugated polymer," Phys. Rev. B, **58**, 7035, (1998).

60. A, Haugeneder, M. Hilmer, C. Kallinger, M. Perner, W. Spirkl, U. Lemmer, J. Feldmann, and U. Svcherf, “Mechanism of gain narrowing in conjugated polymer thin films,” Appl. Phys. B: Lasers and Optics, **66**, 389, (1998).
61. Micheal D. McGehee, and A. J. Heeger, “Semiconducting (conjugated) polymers as materials for solid-state lasers,” Advanced Materials, **12**, 1655, (2000).
62. U. Scherf, S. Riechel, U. Lemmer, and R. F. Mahrt, “Conjugated polymers: lasing and stimulated emission,” Current Opinion in Solid State and Materials Science, **5**, 143, (2001).
63. G. A. Turnbull, P. Andrew, W. L. Barnes, I. D. W. Samuel, “Operating characteristics of a semiconducting polymer laser pumped by a microchip laser,” Appl. Phys. Lett. **82**, 313 (2003).
64. A. Yariv, “Optical electronics in modern communications,” Oxford University Press, (1997).
65. A. Yariv, “*Optical Electronics ,”* Oxford University Press, (1991).
66. G. Kranzelbinder, and G. Leising, “Orgnaic solid-state lasers,” Rep. Prog. Phys. **63**, 729, (2000).
67. H. Kogelnik, and C. V. Shank, “Stimulated emission in a periodic structure,” Appl. Phys. Lett. **18**, 152, (1971).
68. M. D. McGehee, M. A. Diaz-Garcia, F. Hide, R. Gupta, E. K. Miller, D. Moses, and A. J. Heeger, “Semiconducting polymer distributed feedback lasers,” Appl. Phys. Lett. **72**, 1536, (1998).
69. G. Heliotis, R. Xia, D. D. C. Bradley, G. A. Turnbull, I. D. W. Samuel, P. Andrew, and W. L Barnes, “Blue, surface-emitting, distributed feedback polyuorene lasers," Appl. Phys. Lett. **83**, 2118, (2003).
70. R. Xia, G. Heliotis, P. N. Stavrinou, and D. D. C. Bradley, “Polyuorene distributed feedback lasers operating in the green-yellow spectral region," Appl. Phys. Lett. **87**, 031104, (2005).
71. C. Karnutsch, C. Gartner, V. Haug, U. Lemmer, T. Farrell, B. S. Nehls, U. Scherf, J. Wang, T. Weimann, G. Heliotis, C. Pumm, J. C. deMello, and D. D. C. Bradley, “Low threshold blue conjugated polymer laser with first- and second-order distributed feedback," Appl. Phys. Lett. **89**, 201108, (2006).
72. G. A. Turnbull, P. Andrew, M. J. Jory, W. L. Barnes, and I. D. W. Samuel, “Relationship between photonic band structure and emission characteristics of a polymer distributed feedback laser," Phys. Rev. B, **64**, 125122, (2001).
73. J. R. Lawrence, G. A. Tumbull, and I. D. W. Samuel, “Polmyer laser fabricated by a simple micromolding process,” Appl. Phys. Lett. **82**, 4023, (2003).
74. M. Berggren, A. Dodabalapur, R. E. Slusher, A. Timko, and O. Nalamasu, “Organic solid-state lasers with imprinted gratings on plastic substrates,” Appl.

Phys. Lett. **72**, 410, (1998).

75. J. R. Laqrence, P. Andrew, W. L. Bames, M. Buck, G. A. Turnbull, and I. D. W Samuel, "Optical properties of a light-emitting polymer directly patterned by soft lithography," Appl. Phys. Lett. **81**, 1955, (2002).
76. D. Pisignano, L. Persano, P. Visconti, R. Cingolani, G. Gigli, G. Barbarella, and L. Favaretto, "Oligomer-based organic distributed feedback lasers by room-temperature nanoimprint lithography," Appl. Phys. Lett. **83**, 2545, (2003).
77. T. Riedl, T. Rabe, H. H. Johannes, and W. Kowalsky, "Tunable organic thin-film laser pumped by an inorganic violet diode laser," Appl. Phys. Lett. **88**, 241116, (2006).
78. M. A. Diaz-Garcia, F. Hide, B. J. Schwartz, M. D. McGehee, M. R. Andersson, and A. J. Heeger, "Plastic lasers: Comparison of gain narrowing with a soluble semiconducting polymer in waveguides and microcavities," Appl. Phys. Lett. **70**, 3191,(1997).
79. M. Theander, T. Granlund, D. M. Johanson, A. Ruseckas, V. Sundstrom, M. R. Andersson, and O. Inganas, "Lasing in a Microcavity with an oriented liquid-crystalline polyfluorene copolymer as active layer," Adv. Mater. **13**, 323, (2001).
80. V. G. Kozlov, V. Bulovic, P. E. Burrows, M. Baldo, V. B. Khalfin, G. Parthasarathy, S. R. Forrest, Y. You, and M. E. Thompson, "Study of lasing action based on Forster energy transfer in optically pumped organic semiconductor thin films," J. Appl. Phys. **84**, 4096, (1998).
81. T. Virgili, D. G. Lidzey, M. Grell, D. D. C. Bradley, S. Stagira, M. Zavelani-Rossi and S. De Silvestri, "Influence of the orientation of liquid crystalline poly(9,9-dioctylfluorene) on its lasing properties in a planar microcavity," Appl. Phys. Lett. **80**, 4088, (2002).
82. Luana Persano, Pompilio Del Carro, Elisa Mele, Roberto Cingolani,Dario Pisignano, Margherita Zavelani-Rossi, Stefano Longhi and Guglielmo Lanzani, "Monolithic polymer microcavity lasers with on-top evaporated dielectric mirrors," Appl. Phys. Lett. **88**, 121110, (2006).
83. Max Born, and Emil Wolf, "" Principles of Optics," Pergamna Press, (1980).
84. Sebastian Deiries, et al. "Plasma Cleaning", European Southern Observatory, Germany.
85. Ruidong Xia, George Heliotis, Yanbing Hou, and Donal D. C. Bradley, "Fluorene-based conjugated polymer optical gain media," Organic Electronics, 4, **165**, (2003).
86. Mariano Campoy-Quiles, George Heliotis, Ruidong Xia, Marilu Ariu, Martina Pintani, Pablo Etchegoin, and Donal D. C. Bradly, "Ellipsometric Characterization

of the Optical Constants of Polyfluorene Gain Media," Adv. Funct. Mater. **15**, 925, (2005).

87. R. Xia, G. Heliotis, and D. D. C. Bradley, "Fluorene-based polymer gain media for solid-state laser emission across the full visible spectrum," Appl. Phys. Lett. **82**, (2003).
88. T. Smith, and J. Guild, "The C.I.E. colorimetric standards and their use," Trans. Opt. Soc. **33**(3), 73-134 (1931).
89. G. X. Li, S. M. Chen, W. H. Wong, E. Y. B. Pun, and K. W. Cheah, "Highly flexible near-infrared metamaterials," Opt. Express **20**, 397 (2012).
90. Mariano Campoy-Quiles, George Heliotis, Ruidong Xia, Marilu Ariu, Martina Pintani, Pablo Etchegoin, and D. D. C. Bradley, "Ellipsometric characterization of the optical constants of polyfluorene gain media," Adv. Funct. Mater. **15**, 925 (2005).
91. L. A. Coldern, and S. W. Corzine, "Diode Lasers and Photonic Integrated Circuits," Wiley, (1995).
92. https://www.lumerical.com/tcad-products/fdtd/
93. V. Bulovic, V. G. Kozlov, V. B. Khalfin, and S. R. Forrest, "Transform-Limited, Narrow-Linewidth Lasing Action in Organic Semiconductor Microcavities," Science, **279**, 553, (1998).
94. N. Finger, W. Schrenk, and E. Gornik, "Analysis of TM-Polarzied DFB laser structures with metal surface gratings," IEEE Journal of Quantum Electronics, **36**, 7, (2000).

PUBLICATIONS AND CONFERENCE POSTER

Publication

K. L. Chan, G. X. Li, and K. W. Cheah, “Spatially variant color light source using amplified spontaneous emission from organic thin films,” Optical Materials Express, 497, 5, (2015).
(Selection of Spotlight on Optics, The Optical Society, May 2015)

Conference Poster

K. L. Chan, G. X. Li, and K. W. Cheah, “Tunable color emission from cascaded amplified spontaneous emissions in organic thin films,” Poster presentation, 2014 SPIE. Photonics Europe, April 14-17, 2014

CURRICULUM VITAE

Academic qualifications of the thesis author, Mr. CHAN Kin Long,

- Received the degree of Bachelor of Science (Hons.) in Physics (Applied Physics Concentration) from the Hong Kong Baptist University, November 2012.

Aug 2015